# Generalized dynamical phase reduction for stochastic oscillators

Pierre Houzelstein,[1,*] Peter J. Thomas,[2] Benjamin Lindner,[3] Boris Gutkin,[1] and Alberto Pérez-Cervera[4,†]
[1]Group for Neural Theory, LNC2 INSERM U960, DEC, École Normale Supérieure PSL University, Paris, France
[2]Department of Mathematics, Applied Mathematics and Statistics, Case Western Reserve University, Cleveland, Ohio, USA
[3]Bernstein Center for Computational Neuroscience Berlin, D-10115 Berlin, Germany
and Department of Physics, Humboldt Universität zu Berlin, D-12489 Berlin, Germany
[4]Universitat Politècnica de Catalunya, Barcelona, Spain

(Received 5 February 2024; accepted 24 December 2024; published 14 July 2025)

Phase reduction is an important tool for studying coupled and driven oscillators. The question of how to generalize phase reduction to stochastic oscillators remains actively debated. In this work, we propose a method to derive a self-contained stochastic phase equation of the form $\mathrm{d}\phi = a(\phi)\,\mathrm{d}t + \sqrt{2D(\phi)}\,\mathrm{d}W(t)$ that is valid not only for noise-perturbed limit cycles, but also for noise-induced oscillations. We show that our reduction captures the asymptotic statistics of qualitatively different stochastic oscillators, and use it to infer their phase-response properties.

DOI: 10.1103/PhysRevResearch.7.033052

## I. INTRODUCTION

Oscillatory behavior is an ubiquitous phenomenon in physical, biological, chemical, and engineering systems [1]. A powerful way of approaching oscillations is by means of a phase variable. In a purely deterministic system

$$\dot{\mathbf{x}} = \mathbf{F}(\mathbf{x}), \quad \mathbf{x} \in \mathbb{R}^n \tag{1}$$

oscillatory behavior corresponds to stable $T$-periodic solutions of system (1) around the attractor of the dynamics: the limit cycle (LC), which we denote as $\Gamma$. Typically, the existence of the attractor is used to provide a simpler description of the oscillatory dynamics. Namely, one parametrizes the LC, which is a closed curve in the phase space, by means of an angular *phase* variable $\vartheta$ such that $\Gamma = \{\mathbf{x} \,|\, \mathbf{x} = \gamma(\vartheta)\}$. Assuming the solutions are asymptotically close to the limit cycle, the parametrization $\gamma(\vartheta)$ allows one to study the system (1) by means of the *phase reduction*

$$\mathrm{d}\vartheta = \frac{2\pi}{T}\,\mathrm{d}t, \tag{2}$$

which is a one-dimensional description of the periodic dynamics. This phase reduction approach is a well-known method to study complex oscillatory phenomena, such as response to perturbations, phase locking, or synchronization [2,3].

Since real-world systems are often intrinsically fluctuating and noisy, it is natural to aim to extend the phase reduction framework to stochastic oscillators. In principle, a meaningful *stochastic phase reduction* should provide a level of understanding of the dynamics similar to the deterministic case, while incorporating the noisy component observed in realistic oscillations.

A first approach to this question is to consider the noise as a weak perturbation of the LC oscillator [4]. In this case, using a perturbative approach, one can describe the stochastic system by means of the deterministic phase [4–6]. Alternatively, extensions of phase reduction to stochastic systems based on variational methods have been proposed [7,8]. However, perturbative and variational LC approaches both require the existence of an underlying LC. Thus, they have trouble generalizing over the important cases when the addition of noise to a nonoscillatory deterministic system leads to noise-induced oscillations [9].

Therefore, a fundamental challenge for building a general stochastic phase reduction is to define a phase observable that does not require the existence of an underlying LC and that is applicable in the wide range of contexts in which LC and noise-induced oscillations can emerge. Overcoming this challenge in a successful way requires going back to the phase definition itself and updating it. The deterministic phase is defined in terms of two equivalent notions: in terms either of Poincaré sections or of the system's asymptotic behavior [10]. During the last decade, these two notions of phase have been extended to stochastic oscillators. Ten years ago, Schwabedal and Pikovsky [11] found the natural way of extending Poincaré's approach to noisy oscillators. To this end, they constructed a system of isochrons (curves of "equal timing") with the *mean return time property*, namely, that the *average* time it would take a trajectory to complete one oscillation and return to some point on the original isochron should equal the mean period of the oscillator, a criterion that can be also related to the solution of a partial differential equation [12]. As an alternative to the mean-return-time phase, Thomas and

*Contact author: pierre.houzelstein@ens.psl.eu
†Contact author: albert.prz.crv@gmail.com

Lindner proposed that a meaningful phase observable (which they denoted as the "stochastic asymptotic phase") can be extracted from the asymptotic behavior of the conditional density [13].

However, while these two notions of phase solve the problem of finding a phase observable that applies to the many different mechanisms generating stochastic oscillations, a general method for finding a self-contained one-dimensional Markovian phase equation of the form

$$\mathrm{d}\phi = a_\phi(\phi)\,\mathrm{d}t + \sqrt{2D_\phi(\phi)}\,\mathrm{d}W_\phi(t), \tag{3}$$

which approximates the full process, with both $a_\phi$ and $D_\phi$ smooth and periodic in $\phi$, is still missing. While there have been different attempts in the past, they were built *ad hoc* for specific classes of stochastic oscillators [8,14,15].

In this paper, we aim to fill this gap by developing a generalized reduction procedure: given a phase observable $\phi$, we provide a way to obtain a self-contained phase equation as in Eq. (3). We show the generality of our procedure by (1) applying it to two different phase observables (the previously mentioned mean-return-time phase and the stochastic asymptotic phase) and (2) finding self-contained phase equations of qualitatively different noisy oscillators.

Our paper is organized as follows. In Sec. II we introduce the mathematical background, which relies on the spectral decomposition of the Kolmogorov backwards operator $\mathcal{L}^\dagger$. In Sec. III we introduce two different phase observables defined via $\mathcal{L}^\dagger$. Next, in Sec. IV we introduce the main result of this work: the stochastic phase reduction procedure. In Sec. V we introduce two systems in which oscillations emerge from different mechanisms and to which we apply our framework. In Sec. VI we define the asymptotic statistics we use to evaluate the quality of our reduction procedure. In Sec. VII we show a direct application of our framework: predicting the phase-dependent response of the reduced oscillator to an external perturbation. Next, in Sec. VIII we show how our results extend beyond the planar case. We end with a discussion of the results in Sec. IX.

## II. THEORY AND MATHEMATICAL PRELIMINARIES

We assume that the stochastic oscillator is described by a multidimensional Markov process with almost surely continuous sample paths. In particular, we consider the Itô stochastic differential equation (SDE)

$$\mathrm{d}\mathbf{X} = \mathbf{f}(\mathbf{X})\,\mathrm{d}t + \mathbf{g}(\mathbf{X})\,\mathrm{d}\mathbf{W}(t), \tag{4}$$

with $\mathbf{X} \in \mathcal{D} \subset \mathbb{R}^n$ the state vector, and where $\mathbf{W} \in \mathbb{R}^k$ is a collection of IID Wiener processes with increments $\mathrm{d}\mathbf{W}(t)$.

Instead of studying system Eq. (4) by means of individual realizations (a *pathwise* approach), we adopt an *ensemble* perspective: we consider a collection of trajectories described by the conditional probability density function $P(\mathbf{x}, t\,|\mathbf{x_0}, t_0)$. We use the standard convention in which $\mathbf{X}$ refers to the random variable, while $\mathbf{x}$ refers to the independent argument of the corresponding probability density ($\mathbf{X}$ is stochastic whereas $\mathbf{x}$ is a deterministic object).

This density dynamics obeys the Kolmogorov forward (Fokker-Planck) and Kolmogorov backward equations [16]:

$$\frac{\partial}{\partial t}P(\mathbf{x}, t\,|\mathbf{x_0}, t_0) = \mathcal{L}[P] = -\boldsymbol{\nabla}\cdot\mathbf{J}(\mathbf{x}) = -\boldsymbol{\nabla}_{\mathbf{x}}\cdot(\mathbf{f}(\mathbf{x})P) + \boldsymbol{\nabla}^2_{\mathbf{x}}(\mathcal{G}(\mathbf{x})P), \tag{5}$$

$$-\frac{\partial}{\partial t_0}P(\mathbf{x}, t\,|\mathbf{x_0}, t_0) = \mathcal{L}^\dagger[P] = \mathbf{f}^{\mathsf{T}}(\mathbf{x_0})\cdot\boldsymbol{\nabla}_{\mathbf{x_0}}P + \mathcal{G}(\mathbf{x_0})\boldsymbol{\nabla}^2_{\mathbf{x_0}}P, \tag{6}$$

where $\mathcal{G} = \frac{1}{2}\mathbf{g}\mathbf{g}^{\mathsf{T}}$. In Eq. (5), we introduced $\mathbf{J}(\mathbf{x})$, the probability current

$$\mathbf{J}(\mathbf{x}) = \mathbf{f}(\mathbf{x})P - \boldsymbol{\nabla}_{\mathbf{x}}\cdot(\mathcal{G}(\mathbf{x})P), \tag{7}$$

which allows us to naturally introduce boundary conditions for the operator $\mathcal{L}$ in the domain $\mathcal{D}$ as

$$\mathbf{n}\cdot\mathbf{J}(\mathbf{x}) = 0, \qquad \mathbf{x} \in \partial\mathcal{D}, \tag{8}$$

with $\boldsymbol{n}$ the normal vector to the boundary. This ensures the total probability density is preserved. The boundary conditions for $\mathcal{L}^\dagger$ are adjoint to those of $\mathcal{L}$ and write as

$$(\mathcal{G}(\mathbf{x})\cdot\boldsymbol{\nabla}_{\mathbf{x}}F(\mathbf{x}))\cdot\mathbf{n} = 0. \tag{9}$$

The backward operator $\mathcal{L}^\dagger$ in (6) is known as the generator of the Markov process $\mathbf{X}(t)$ and is the infinitesimal generator of the family of stochastic Koopman operators associated with Eq. (4) [17,18]. If we define the Koopman semigroup of operators $\mathcal{K}^{\Delta t}$ acting on a real valued observable $F(\mathbf{x})$ of system (4) such that

$$\mathcal{K}^{\Delta t}[F(\mathbf{x}(t))] = \langle F(\mathbf{x}(t+\Delta t))\rangle, \tag{10}$$

then [18]

$$\mathcal{L}^\dagger[F] = \lim_{\Delta t\to 0}\frac{\mathcal{K}^{\Delta t}[F(\mathbf{x}(t))] - F(\mathbf{x}(t))}{\Delta t}. \tag{11}$$

We assume that the forward ($\mathcal{L}$) and backward ($\mathcal{L}^\dagger$) Kolmogorov operators possess a discrete spectrum with a one-dimensional null space, and eigenvalues $\lambda$ and eigenfunctions $P_\lambda, Q^*_\lambda$ satisfying

$$\mathcal{L}[P_\lambda] = \lambda P_\lambda, \quad \mathcal{L}^\dagger[Q^*_\lambda] = \lambda Q^*_\lambda. \tag{12}$$

Biorthogonality of the eigenfunctions under the natural inner product follows:

$$\langle Q_{\lambda'}\,|\,P_\lambda\rangle = \int d\mathbf{x}\, Q^*_{\lambda'}(\mathbf{x})P_\lambda(\mathbf{x}) = \delta_{\lambda'\lambda}. \tag{13}$$

This relation allows us to decompose the conditional probability density as follows [16]: for $t > t_0$,

$$P(\mathbf{x}, t\,|\mathbf{x_0}, t_0) = P_0(\mathbf{x}) + \sum_{\lambda\neq 0} e^{\lambda(t-t_0)}P_\lambda(\mathbf{x})Q^*_\lambda(\mathbf{x_0}), \tag{14}$$

where $P_0$ is the eigenfunction associated with eigenvalue 0. Properly normalized, it gives the stationary probability density, which in turn defines a stationary density current $\mathbf{J}_0(\mathbf{x})$. As we are considering stochastic oscillatory systems, which are out of detailed balance, we assume $\mathbf{J}_0(\mathbf{x})$ to be non-vanishing.

According to Itô's chain rule [16,17], for any smooth ($C^2$) observable $F(\mathbf{X})$

$$dF(\mathbf{X}) = \mathcal{L}^\dagger[F(\mathbf{X})]\,\mathrm{d}t + \nabla F(\mathbf{X})^\intercal \mathbf{g}(\mathbf{X})\,\mathrm{d}\mathbf{W}(t). \tag{15}$$

Thus, for any stochastic process, the ensemble properties and pathwise realizations of the system are linked through the Kolmogorov backwards operator.

## III. ESTABLISHED PHASE MAPPINGS

The second-order differential operator $\mathcal{L}^\dagger$ has been used to define two distinct notions of phase reduction for stochastic oscillators, which do not require the existence of an underlying LC: the stochastic asymptotic phase $\Psi(\mathbf{x})$, based on the spectral decomposition of the operator [13], and the mean-return-time phase $\Theta(\mathbf{x})$ [11], which is defined in terms of a mean first-passage time problem involving the same operator $\mathcal{L}^\dagger$ [12]. While these two notions of phase, detailed below, arise from the same operator $\mathcal{L}^\dagger$, they are formally and quantitatively distinct [19]. Nevertheless, in the case of a system consisting of a LC perturbed by noise, both mappings, $\Psi(\mathbf{x})$ and $\Theta(\mathbf{x})$, converge to the deterministic asymptotic phase $\vartheta(\mathbf{x})$ in the limit of small noise [12,20,21].

### A. The stochastic asymptotic phase

Consider system (4) and its associated decomposition of $P(\mathbf{x}, t|\mathbf{x}_0, t_0)$ (14). As proposed in Ref. [13], if the spectrum of $\mathcal{L}^\dagger$ fulfills the following heuristic conditions:

(1) There exists a nontrivial eigenvalue of $\mathcal{L}^\dagger$ with least negative real part $\lambda_1 = \mu_1 + i\omega_1$, which is complex valued ($\omega_1 > 0$) and unique

(2) The oscillation is pronounced, i.e., the *quality factor* $|\omega_1/\mu_1|$ is much larger than 1

(3) All other nontrivial eigenvalues $\lambda'$ are significantly more negative in their real parts, i.e., $|\mathrm{Re}[\lambda']| \geqslant 2|\mathrm{Re}[\lambda_1]|$

then the approach to the stationary distribution $P_0(\mathbf{x})$ from Eq. (14) is dominated by a long-lived oscillatory mode $e^{\lambda_1(t-t_0)}P_{\lambda_1}(\mathbf{x})Q^*_{\lambda_1}(\mathbf{x}_0) + \mathrm{c.c.}$, even after all other modes in Eq. (14) have decayed [22]. Appendix A provides examples of different spectra with such structure. As discussed in [13], the argument $\Psi(\mathbf{x})$ of the complex backward eigenfunction $Q^*_{\lambda_1}$,

$$Q^*_{\lambda_1}(\mathbf{x}) = u(\mathbf{x})e^{i\Psi(\mathbf{x})}, \tag{16}$$

is the natural generalization of the deterministic asymptotic phase: at large times, and provided the previous set of conditions (denoted in [13] as the *robustly oscillatory* criterion) is met, if one considers the same system at initial time $t = t_0$ with two different initial conditions $[\mathbf{x}(t_0) = \mathbf{x}_1]$ and $[\mathbf{x}(t_0) = \mathbf{x}_2]$, the respective probability densities $P(\mathbf{y}, t|\mathbf{x}_1, t_0)$ and $P(\mathbf{y}, t|\mathbf{x}_2, t_0)$ will decay to the stationary state with an oscillatory offset given by $\Psi(\mathbf{x}_1) - \Psi(\mathbf{x}_2)$. Thus, $\Psi(\mathbf{x})$ defines level sets,

$$\mathcal{I}_\psi(\mathbf{x}) = \{\mathbf{x} \,|\, \Psi(\mathbf{x}) = \psi\}, \tag{17}$$

corresponding to the sets of initial conditions such that the main oscillatory component of their conditional probability densities will evolve in phase with each other. For this reason, $\Psi(\mathbf{x})$ was denoted in [13] as the *stochastic asymptotic phase*.

Applying the Itô chain rule to this new observable $\Psi(\mathbf{x})$, we extract its evolution law [19]

$$\mathrm{d}\Psi(\mathbf{X}) = \left(\omega_1 - \overbrace{2\sum_{i,j}\mathcal{G}_{ij}(\mathbf{X})\partial_i \ln(u(\mathbf{X}))\partial_j\Psi(\mathbf{X})}^{\Omega(\mathbf{X})}\right)\mathrm{d}t + \nabla\Psi(\mathbf{X})^\intercal\mathbf{g}(\mathbf{X})\mathrm{d}\mathbf{W}(t), \tag{18}$$

where we introduce the function $\Omega(\mathbf{x})$ to ease notation.

### B. The mean-return-time stochastic phase

An alternative definition for the phase of stochastic oscillators was proposed by Schwabedal and Pikovsky in [11], who constructed the *mean-return-time phase* in terms of a system of Poincaré sections, which we write $\ell_{\mathrm{MRT}}(\varphi)$, with $0 \leqslant \varphi \leqslant 2\pi$, foliating a domain $\mathcal{R} \subset \mathbb{R}^2$ and possessing a mean-return-time (MRT) property: a section $\ell_{\mathrm{MRT}}$ satisfies the MRT property if for all the points $\mathbf{x} \in \ell_{\mathrm{MRT}}$ the mean return time $\overline{T}$ from $\mathbf{x}$ back to $\ell_{\mathrm{MRT}}$, having completed one full rotation, is constant.

First constructed in [11] by means of an algorithmic numerical procedure, the MRT phase was later related to the solution of a boundary value problem in [12], in which it was shown that the $\ell_{\mathrm{MRT}}$ sections correspond to the level curves of a function $T(\mathbf{x})$ satisfying the following PDE associated with a first-passage-time problem:

$$\mathcal{L}^\dagger[T(\mathbf{x})] = -1, \tag{19}$$

where $\mathcal{L}^\dagger$ corresponds to the Kolmogorov backwards operator defined in Eq. (6) [23]. Imposing a boundary condition amounting to a jump by $\overline{T}$ across an arbitrary section transverse to the oscillation [24], the *unique* solution of Eq. (19), up to an additive constant $T_0$, is a version of the so-called MRT function,

$$\Theta(\mathbf{x}) = (2\pi/\overline{T})[T_0 - T(\mathbf{x})]. \tag{20}$$

Combining (19) and (20), the MRT phase $\Theta(\mathbf{x})$ satisfies

$$\mathcal{L}^\dagger[\Theta(\mathbf{x})] = \frac{2\pi}{\overline{T}}, \tag{21}$$

and the transformation of $\mathbf{X}(t)$ in Eq. (4) to the MRT phase $\Theta$ obeys the stochastic differential equation

$$\mathrm{d}\Theta(\mathbf{X}) = \frac{2\pi}{\overline{T}}\mathrm{d}t + \nabla\Theta(\mathbf{X})^\intercal\mathbf{g}(\mathbf{X})\mathrm{d}\mathbf{W}(t), \tag{22}$$

so its mean evolves in a way which is formally analogous to the dynamics for the deterministic phase [see Eq. (2)].

## IV. SELF-CONTAINED PHASE EQUATION

We have introduced two different phase mappings: the asymptotic phase $\Psi(\mathbf{x})$ and the MRT phase $\Theta(\mathbf{x})$, which yield two different equations, (18) and (22), respectively. However, neither of these equations is fully self-contained, as they both depend on $\mathbf{X}(t)$ [25].

Given an arbitrary phase mapping

$$\Phi : \mathcal{D} \subset \mathbb{R}^n \to \mathbb{T}$$
$$\mathbf{x} \to \Phi(\mathbf{x}), \tag{23}$$

so the evolution of the phase observable $\Phi(\mathbf{X}(t))$ follows

$$\mathrm{d}\Phi(\mathbf{X}) = \mathcal{L}^{\dagger}[\Phi(\mathbf{X})]\,\mathrm{d}t + \nabla\Phi(\mathbf{X})^{\intercal}\mathbf{g}(\mathbf{X})\,\mathrm{d}\mathbf{W}(t), \tag{24}$$

we aim to derive a reduction procedure leading to a self-contained equation of the form

$$\mathrm{d}\phi = a_{\phi}(\phi)\,\mathrm{d}t + \sqrt{2D_{\phi}(\phi)}\,\mathrm{d}W_{\phi}(t), \tag{25}$$

where $\mathrm{d}W_{\phi}$ is the increment of a single Brownian motion (rather than $k$ of them) and $D_{\phi}$ is a (phase-dependent) effective noise intensity. Both $D_{\phi}$ and the phase-dependent local frequency $a_{\phi}$ should be smooth and periodic in $\phi$ [such that $a_{\phi}(\phi) = a_{\phi}(\phi + 2\pi)$ and $D_{\phi}(\phi) = D_{\phi}(\phi + 2\pi)$]. While Eq. (25) is a fully self-contained phase equation, it presents the challenge of estimating these new functions $a_{\phi}(\phi)$ and $D_{\phi}(\phi)$ in such a way the reduced and self-contained dynamics $\phi(t)$ in (25) approximate as precisely as possible the full phase dynamics $\Phi[\mathbf{X}(t)]$ in (24).

### A. Phase mapping requirements

For our reduction procedure, we need the phase mapping $\Phi(\mathbf{x})$ in (23) to satisfy the following set of conditions. We assume $\Phi(\mathbf{x})$ to uniquely assign a single and well-defined phase to each point $\mathbf{x} \in \mathcal{D}$ and to be continuous (at least $C^2$). In this way, we assume it is possible to parametrize phase level sets (the *isochrons*) by means of a set $\boldsymbol{\eta} = (\eta_1, \ldots, \eta_{n-1})$ of $n-1$ amplitude-like variables, with $\eta_i(\mathbf{x}) \in \mathbb{R} \quad \forall i \in \{1, \ldots, n-1\}$. This requirement amounts to assuming the existence of an *invertible* parametrization $\mathbf{x} = K(\phi, \boldsymbol{\eta})$:

$$\begin{aligned} K : \mathbb{T} \times \mathbb{R}^{n-1} &\to \mathcal{D} \subset \mathbb{R}^n \\ (\phi, \boldsymbol{\eta}) &\to K(\phi, \boldsymbol{\eta}) \end{aligned} \tag{26}$$

with $K(\phi, \boldsymbol{\eta}) = K(\phi + 2\pi, \boldsymbol{\eta})$. We remark that since the phaseless sets (i.e, the points in which the phase function is not defined) are not invertible, neither they nor a small $\epsilon$-ball around them can belong to the domain $\mathcal{D}$. Thus the isochrons provide a foliation of the domain, $\mathcal{D} = \bigcup_{\phi\in[0,2\pi)} \mathcal{I}_{\phi}$, where the $\mathcal{I}_{\phi}$ are nonempty, simply connected, and pairwise disjoint.

### B. Reduction framework

Consider the general phase observable $\Phi(\mathbf{x})$ in Eq. (23), and assume the conditions given in Sec. IV A are satisfied. Given that the sum of uncorrelated Gaussian white noise processes is Gaussian white noise, we rewrite Eq. (24) with one-dimensional Gaussian white noise $\mathrm{d}W_{1\mathrm{D}}$, such that

$$\mathrm{d}\Phi(\mathbf{X}) = \mathcal{L}^{\dagger}[\Phi(\mathbf{X})]\,\mathrm{d}t + \sqrt{2D(\mathbf{X})}\,\mathrm{d}W_{1\mathrm{D}}, \tag{27}$$

where the new noise amplitude term is given by

$$D(\mathbf{x}) = \frac{1}{2}\sum_{ijk} g_{ij}(\mathbf{x})g_{kj}(\mathbf{x})\partial_i\Phi(\mathbf{x})\partial_k\Phi(\mathbf{x}).$$

In what follows, we show a way in which the system in Eq. (27) can be approximated by a reduced, self-contained equation of the form in Eq. (25). In a nutshell, we rely on the existence of the invertible transformation $\mathbf{x} = K(\phi, \boldsymbol{\eta})$ in (26) to integrate out the $n-1$ transverse directions, leaving only the phase dependency. For simplicity, we assume that we are in the planar case ($n = 2$), so we only have one transverse variable, $\eta_1 = \eta$, to integrate out.

To start, we rewrite the stationary probability density $P_0(\mathbf{x})$ in terms of this new set of coordinates $\mathbf{x} = K(\phi, \eta)$, and obtain the distribution $\bar{P}_0(\phi, \eta)$. We use it to define the following *conditional* probability

$$\bar{P}_0(\eta|\phi) \equiv \frac{\bar{P}_0(\phi, \eta)}{\bar{P}_0(\phi)}, \tag{28}$$

provided the density $\bar{P}_0(\phi) > 0$, $\forall\,\phi \in \mathbb{T}$. Note that $K(\phi, \eta) = K(\phi + 2\pi, \eta)$, implying $\bar{P}_0(\eta|\phi) = \bar{P}_0(\eta|\phi + 2\pi)$.

Consider the dynamics for $\mathrm{d}\Phi(\mathbf{X})$ in Eq. (27). If we take the expected value of each side, using the stationary probability density, since $\mathrm{d}W_{1D}(t)$ is independent of $\mathbf{X}(t)$ [and functions of $\mathbf{X}(t)$], we see that $\langle\sqrt{2D(\mathbf{X}(t))}\,\mathrm{d}W_{1D}\rangle \equiv 0$. This motivates our choice of $a_{\phi}(\phi)$: we want $a_{\phi}(\phi)$ to represent the average rate of increase of $\Phi(\mathbf{X}(t))$ when $\mathbf{X}(t)$ happens to be on a particular isochron; that is,

$$a_{\phi}(\phi) = \int_{\mathbf{x}\in\mathcal{I}_{\phi}} \mathcal{L}^{\dagger}[\Phi(\mathbf{x}(\phi, \eta))]\bar{P}_0(\eta|\phi)\,d\eta, \tag{29}$$

where $\mathcal{L}^{\dagger}[\Phi(\mathbf{x}(\phi, \eta))]$ is the drift of $\Phi(\mathbf{x})$ in Eq. (24), which is averaged over the level curves of $\Phi(\mathbf{x})$,

$$\mathcal{I}_{\phi} = \{\mathbf{x} \in \mathcal{D} | \Phi(\mathbf{x}) = \phi\},$$

which we parametrize by means of the transverse coordinate $\eta$. The $2\pi$ periodicity of both $K(\phi, \eta)$ and $\bar{P}_0(\eta|\phi)$ in $\phi$ implies $a_{\phi}(\phi) = a_{\phi}(\phi + 2\pi)$.

The choice of $a_{\phi}(\phi)$ in Eq. (29) is meant to ensure that our reduction captures the first moment of the short-term dynamics of $\Phi(\mathbf{X}(t))$. Assuming stationarity, Eq. (29) is equivalent to

$$a_{\phi}(\phi) = \lim_{\mathrm{d}t\to 0} \frac{1}{\mathrm{d}t}\langle\Delta\Phi(\mathbf{X}(t))\rangle_{\Phi(\mathbf{X}(t))=\phi} \tag{30}$$

with

$$\Delta\Phi(\mathbf{X}(t)) = \Phi_{\mathrm{unwrapped}}(\mathbf{X}(t + \mathrm{d}t)) - \Phi_{\mathrm{unwrapped}}(\mathbf{X}(t)), \tag{31}$$

the increment of the phase variable between $t$ and $t + \mathrm{d}t$. Computing phase increments requires omitting phase resets at $2\pi$. This is why we introduce $\Phi_{\mathrm{unwrapped}}(\mathbf{x})$, which maps $\mathbf{x}$ onto the real line $\mathbb{R}$ instead of the circle $\mathbb{T}$, such that

$$\Phi(\mathbf{x}) = \Phi_{\mathrm{unwrapped}}(\mathbf{x}) \mod 2\pi.$$

Once our choice of $a_{\phi}(\phi)$ is thus made, we choose $D_{\phi}(\phi)$ such that we best capture the second moment of the short-term dynamics of the phase:

$$D_{\phi}(\phi) = \lim_{\mathrm{d}t\to 0} \frac{1}{2\,\mathrm{d}t}\left\langle[\Delta\Phi(\mathbf{X}(t)) - a_{\phi}(\phi)\,\mathrm{d}t]^2\right\rangle_{\Phi(\mathbf{X}(t))=\phi}. \tag{32}$$

Expanding this formula yields

$$D_{\phi}(\phi) = \frac{1}{2}\sum_{ijk}\int_{\mathbf{x}\in\mathcal{I}_{\phi}} g_{ij}(\mathbf{x})g_{kj}(\mathbf{x})\partial_i\Phi(\mathbf{x})\partial_j\Phi(\mathbf{x})\bar{P}_0(\eta|\phi)\,d\eta, \tag{33}$$

where again $\mathbf{x} = K(\phi, \eta)$. Using the same argument as for $a_{\phi}$, we find $D_{\phi}(\phi) = D_{\phi}(\phi + 2\pi)$.

Finally, we note that using Eqs. (30) and (32) make it possible to extract $a_{\phi}$ and $D_{\phi}$ from a stationary time series $\Phi(\mathbf{X}(t))$. They are obtained as the first two Kramers-Moyal

coefficients of the trajectory $\phi(t)$. See [26–28] for examples of how to extract them from stochastic trajectories, and the Supplemental Material (SM) [29] for numerical details.

### C. Stochastic asymptotic phase reduction

Let us now apply the general framework derived above to obtain a reduced evolution equation for the stochastic asymptotic phase, of the form

$$\mathrm{d}\psi = a_\psi(\psi)\,\mathrm{d}t + \sqrt{2D_\psi(\psi)}\,\mathrm{d}W_\psi(t). \tag{34}$$

From Eq. (18), we find that the drift term takes the form

$$a_\psi(\psi) = \omega_1 - \int_{\mathbf{x}\in\mathcal{I}_\psi} \bar{P}_0(\eta|\psi)\Omega(\mathbf{x}(\psi,\eta))\,d\eta.$$

Similarly, the effective noise term takes the form

$$D_\psi(\psi) = \frac{1}{2}\sum_{ijk}\int_{\mathbf{x}\in\mathcal{I}_\psi} g_{ij}(\mathbf{x})g_{kj}(\mathbf{x})\partial_i\Psi(\mathbf{x})\partial_j\Psi(\mathbf{x})\bar{P}_0(\eta|\psi)\,d\eta, \tag{35}$$

where $\mathbf{x} = K(\psi,\eta)$ and $\mathcal{I}_\psi$ refers to

$$\mathcal{I}_\psi = \{\mathbf{x}|\Psi(\mathbf{x}) = \psi\}.$$

As noted previously, under the stationarity assumption, those two expressions can be approximated from time series realizations of $\Psi(\mathbf{X}(t))$ using Eqs. (30) and (32).

### D. Mean-return-time phase reduction

Let us now derive a reduced phase equation for the mean-return-time phase, of the form

$$\mathrm{d}\theta = a_\theta(\theta)\,\mathrm{d}t + \sqrt{2D_\theta(\theta)}\,\mathrm{d}W_\theta(t). \tag{36}$$

Following the same general reduction procedure, we obtain expressions for the corresponding drift function,

$$a_\theta(\theta) = \frac{2\pi}{\overline{T}}, \tag{37}$$

and the effective noise function,

$$D_\theta(\theta) = \sum_{i,j}\int_{\mathbf{x}\in\mathcal{I}_\theta} \bar{P}_0(\eta|\theta)\partial_i\Theta(\mathbf{x})\partial_j\Theta(\mathbf{x})\mathcal{G}_{ij}(\mathbf{x})\,d\eta, \tag{38}$$

where $\mathbf{x} = K(\theta,\eta)$, and $\mathcal{I}_\theta$ accounts for the MRT sections

$$\mathcal{I}_\theta = \{\mathbf{x}|\Theta(\mathbf{x}) = \theta\}.$$

## V. NUMERICAL SIMULATIONS

We apply our framework to two 2D systems exhibiting canonical bifurcations and illustrating various mechanisms of noisy oscillations. We use a finite-differences scheme to compute the stochastic asymptotic phase $\Psi(\mathbf{x})$ and the MRT phase $\Theta(\mathbf{x})$, as well as the stationary density $P_0(\mathbf{x})$, and Eq. (30) and Eq. (32) to obtain the drift functions $a_\psi$, $a_\theta$ and the diffusion functions $D_\psi$, $D_\theta$. We refer the reader to the SM [29] for the complete numerical details.

### A. Noisy Hopf bifurcation

We consider the canonical model for a supercritical Hopf bifurcation endowed with Gaussian white noise:

$$\begin{aligned}\mathrm{d}X &= [(\delta-\kappa R^2)X - (\gamma-\beta R^2)Y]\,\mathrm{d}t + \sqrt{2D}\,\mathrm{d}W_x(t),\\ \mathrm{d}Y &= [(\gamma-\beta R^2)X + (\delta-\kappa R^2)Y]\,\mathrm{d}t + \sqrt{2D}\,\mathrm{d}W_y(t),\end{aligned} \tag{39}$$

$R = \sqrt{X^2+Y^2}$. In what follows, $\beta = 0.5$, $\gamma = 4$, $\kappa = 1$ [30]. In the deterministic setting, there is a supercritical Hopf bifurcation at $\delta = 0$. For $\delta > 0$, there is a stable limit cycle $\Gamma$ of radius $R_* = \sqrt{\delta/\kappa}$ and period $T = \frac{2\pi}{\gamma-\beta R_*^2}$, which can be parameterized using the phase function $\vartheta(x,y) = \arctan(y/x) - \frac{\beta}{\kappa}\log\frac{r}{R_*}$ [30]. The stochastic version has been studied for a long time, especially with respect to its correlation statistics (see, e.g., [31–33]), and, more recently, by means of the spectrum of $\mathcal{L}^\dagger$ [30].

In Fig. 1 we show properties of the noisy system above the bifurcation ($\delta = 1$). We observe that, as we are considering additive isotropic noise, the phase functions $\Psi(\mathbf{x})$ and $\Theta(\mathbf{x})$ still exhibit the characteristic rotationally invariant rectilinear structure modulated by the "twist factor" $\beta/\kappa$ that would be present without noise [30] (see Fig. 1, panels 1.a and 2.a and 1.b and 2.b). Figure 1 panels 1.c and 2.c show that the stationary probability densities $P_0(\mathbf{x})$ preserve the radial symmetry for low and high noise amplitude ($D = 0.01$ and $D = 0.08$, respectively), thus indicating that the trajectories are dispersed around the LC in a radially symmetric way, spreading increasingly with the level of noise. Hence, the constant drift and effective diffusion terms we recover (see Fig. 1, panels 1.d and 2.d) follow from the rotational symmetry of all the terms in (29) and (33).

Next, we consider the case below the bifurcation but close to it ($\delta = -0.01$) because of its interest in applications, such as in neuroscience [34]. In this case, the deterministic system has a stable focus at the origin. Hence, in the absence of noise, the trajectories exhibit damped oscillations decaying towards the origin, and the asymptotic phase is not well defined [35]. The addition of noise perturbs trajectories away from the stable steady state, leading to quasicycle oscillations [14,36]. This is an example of noise-induced oscillations, leading to a nonzero probability of finding the system away from that fixed point. As can be seen in Fig. 2(c), the probability density has a 2D Gaussian-like profile, the maximum of which is located at the origin, where the deterministic fixed point is found. Despite the noise-induced character of the oscillation, the phase functions $\Psi(\mathbf{x})$ and $\Theta(\mathbf{x})$ have a structure similar to those of the LC case [Figs. 2(a) and 2(b)]. As in the noisy LC case, the rotational symmetry of both $P_0$ and the phase mappings yields constant drift and effective noise functions (Fig. 2, panels 1.d and 2.d). However, we note that for the same levels of noise, the effective noise intensities $D_\psi$ and $D_\theta$ are much larger than in the LC case.

### B. Saddle node on an invariant circle

Next, we consider a system that undergoes a saddle-node bifurcation on an invariant circle (SNIC) in the deterministic

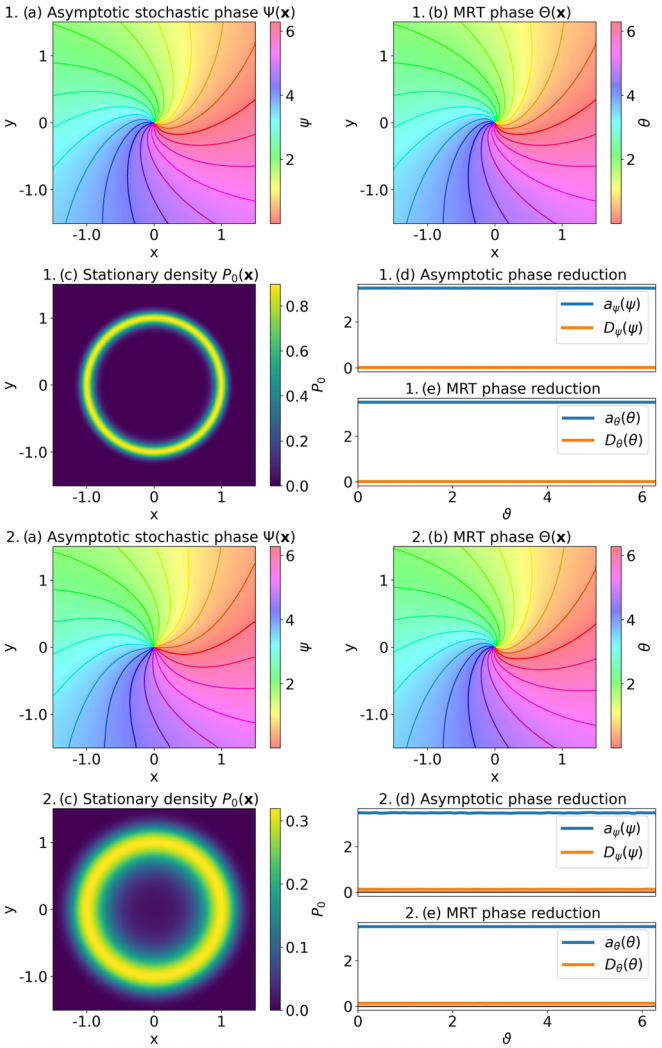


FIG. 1. Hopf above bifurcation. For the noisy Hopf bifurcation model in Eq. (39) with $\delta = 1$, $\beta = 0.5$, $\gamma = 4$, $\kappa = 1$, we show for two levels of noise (panel 1, above $D = 0.01$ and panel 2, below $D = 0.08$). (a) The asymptotic phase function $\Psi(\mathbf{x})$. (b) The MRT phase function $\Theta(\mathbf{x})$. (c) The stationary probability distribution. (d) Top panel shows the functions $a_\psi$ and $D_\psi$, and bottom panel shows $a_\theta$ and $D_\theta$, abscissa shared.

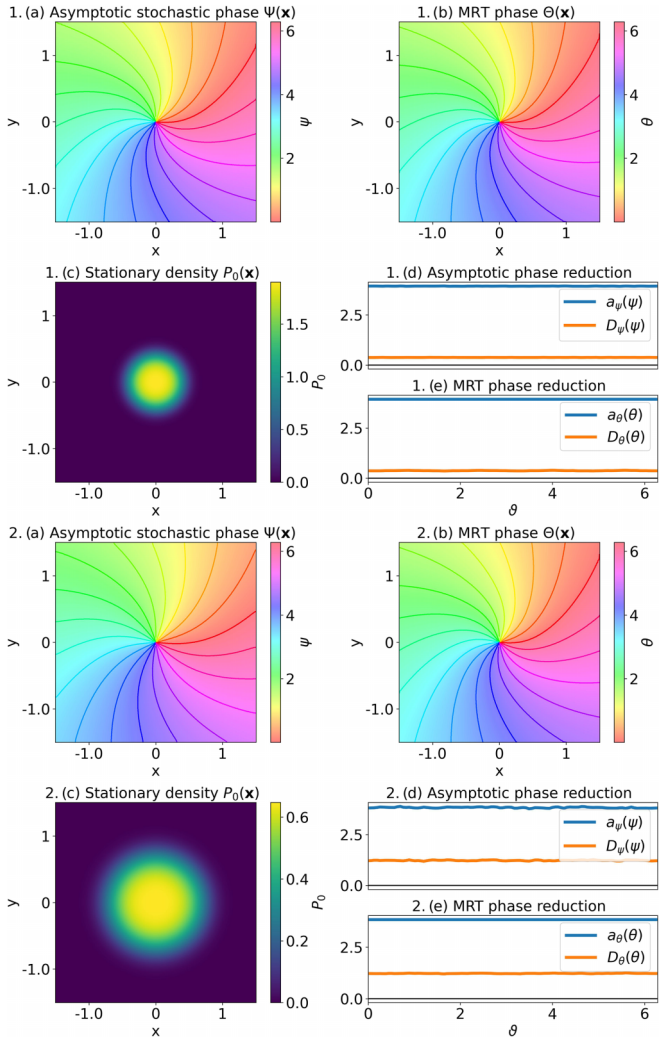


FIG. 2. Hopf below bifurcation. For the noisy Hopf bifurcation model in Eq. (39) with $\delta = -0.01$, $\beta = 0.5$, $\gamma = 4$, $\kappa = 1$, we show for two levels of noise (panel 1, above $D = 0.01$ and panel 2, below $D = 0.08$). (a) The asymptotic phase function $\Psi(\mathbf{x})$. (b) The MRT phase function $\Theta(\mathbf{x})$. (c) The stationary probability distribution. (d) Top panel shows the functions $a_\psi$ and $D_\psi$, and bottom panel shows $a_\theta$ and $D_\theta$, abscissa shared.

regime:

$$\begin{aligned} dX &= \left[nX - mY - XR^2 + \frac{Y^2}{R}\right] dt + \sqrt{2D}\, dW_x(t), \\ dY &= \left[mX + nY - YR^2 - \frac{XY}{R}\right] dt + \sqrt{2D}\, dW_y(t), \end{aligned} \tag{40}$$

where $R(X, Y) = \sqrt{X^2 + Y^2}$, with $m, n \in \mathbb{R}$. We fix $n = 1$, so in the noiseless case, there is an invariant curve $\Gamma$ of radius $\sqrt{n} = 1$. When $m < 1$, there are two fixed points onto $\Gamma$, a saddle and a node, which collide at $m = 1$, thus yielding an oscillatory LC state for $m > 1$. The addition of noise to the saddle-node regime induces a nonzero probability that the system will leave the stable point and jump onto the circle, leading to oscillations. We refer to this state as the *excitable* regime of the system.

Let us now present how our phase reduction applies to system Eq. (40) in the oscillatory ($m = 1.03$) and excitable cases ($m = 0.999$). In the low noise case (panel 1 in Figs. 3 and 4, for the oscillatory and excitable regimes, respectively), we observe the phase functions $\Psi(\mathbf{x})$ and $\Theta(\mathbf{x})$ to have a similar structure reflecting the asymmetries in the velocity of the system during a cycle. As the trajectories slow down near the ghost of the saddle node, the phase sections appear more densely packed in this area of the phase space. These velocity variations seem to be reflected in the drift term of the asymptotic phase reduction $a_\psi$: both above and below the bifurcation and for small and large noise values, we observe $a_\psi$ to be smaller (larger) near to (far from) the phase values corresponding to the locations of the saddle node (see panels 1.d and 2.d in Figs. 3 and 4).

A closer look at our results reveals that for small levels of noise and below the bifurcation, the asymptotic phase drift $a_\psi$

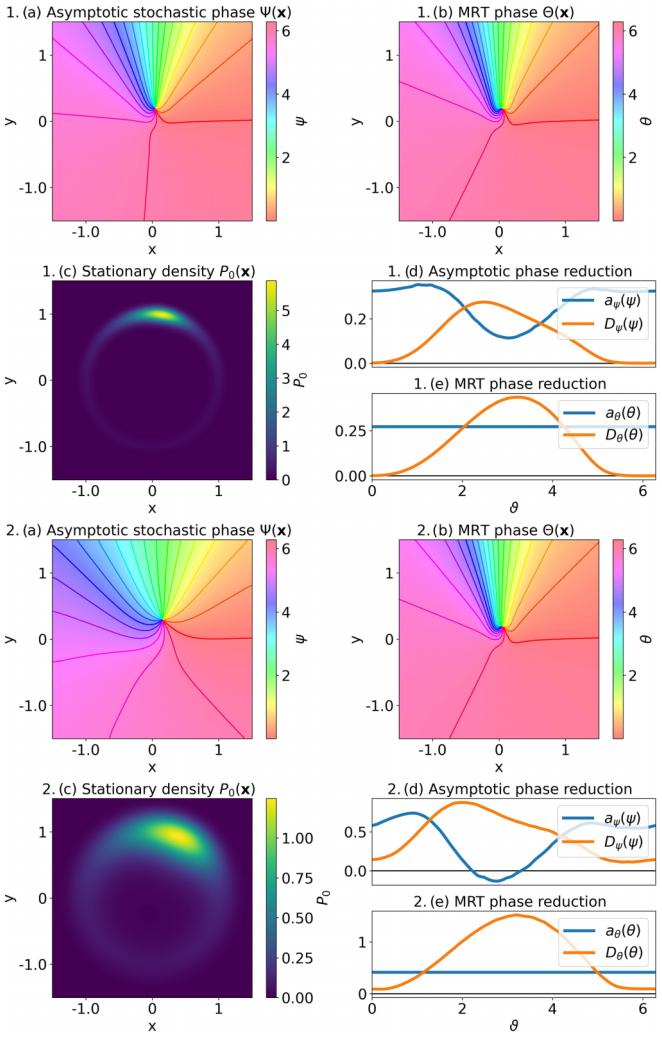


FIG. 3. SNIC above bifurcation. For the noisy SNIC bifurcation model in Eq. (40) with $n = 1$, $m = 1.03$ we show for two levels of noise (panel 1, above $D = 0.01$ and panel 2, below $D = 0.08$). (a) The asymptotic phase function $\Psi(\mathbf{x})$. (b) The MRT phase function $\Theta(\mathbf{x})$. (c) The stationary probability distribution. (d) Top panel shows the functions $a_\psi$ and $D_\psi$, and bottom panel shows $a_\theta$ and $D_\theta$, abscissa shared.

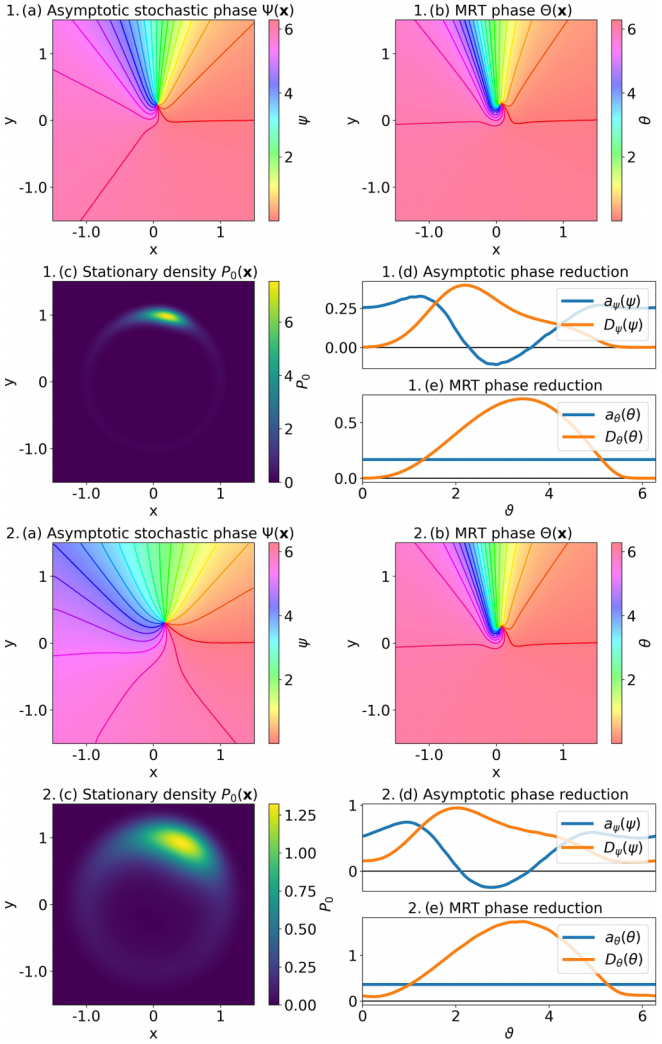


FIG. 4. SNIC below bifurcation. For the noisy SNIC bifurcation model in Eq. (40) with $n = 1$, $m = 0.999$ we show for two levels of noise (panel 1, above $D = 0.01$, and panel 2, below $D = 0.08$). (a) The asymptotic phase function $\Psi(\mathbf{x})$. (b) The MRT phase function $\Theta(\mathbf{x})$. (c) The stationary probability distribution. (d) Top panel shows the functions $a_\psi$ and $D_\psi$, and bottom panel shows $a_\theta$ and $D_\theta$, abscissa shared.

shows two zero crossings (Fig. 4, panel 1.d). Indeed, there is a phase interval for which the drift term $a_\psi$ becomes negative: in that range, the phase $\psi$ behaves like a particle stuck in a one-dimensional potential well and subjected to thermal fluctuations with noise intensity $D_\psi(\psi)$. A full rotation occurs when the fluctuations manage to push the phase out of the well. Furthermore, we observe that, if we keep the noise weak and $m$ is varied so that the system goes above the bifurcation, $a_\psi$ becomes fully positive (Fig. 3, panel 1.d). We check in Fig. 5 that this transition seems to be continuous, as the drift appears to smoothly move across the zero line as the bifurcation parameter $m$ is taken across $m = 1$. By contrast, this transition across the zero line as the $m$ parameter is varied around 1 does not hold anymore when noise levels get too large. Indeed, looking at Figs. 3 and 4, panels 2, the drift terms $a_\psi$ show zero crossings both below and above the bifurcation. In Appendix B, we provide additional details about the speed

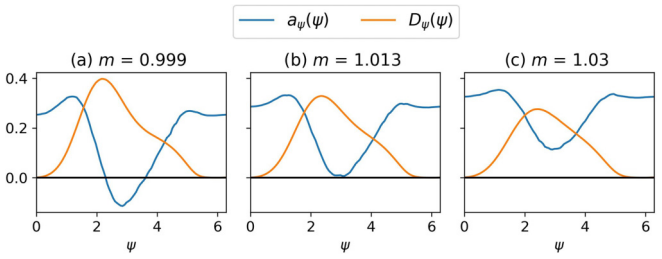


FIG. 5. Transition across the SNIC bifurcation. Asymptotic stochastic phase $\psi$ drift function $a_\psi(\psi)$ (blue) and effective diffusion term $D_\psi(\psi)$ (orange) for the SNIC for $n = 1$, $D = 0.01$, and increasing values of $m$ across the bifurcation ($y$ axis shared). The transition from excitable to oscillatory regime appears to be reflected in the presence or absence of crossings in the drift function and in the decrease of the noise amplitude term. (a) $m = 0.999$; (b) $m = 1.013$; (c) $m = 1.03$.

variations of the drift term $a_\psi$ and the emergence of zero crossings above the bifurcation as the noise is increased.

The interplay of deterministic and stochastic effects is apparent in the shape of the effective noise function $D_\psi$. In contrast to the previously studied rotational invariant Hopf case, now the asymmetries in both $\Psi(\mathbf{x})$ and $P_0(\mathbf{x})$ lead to a nonconstant function $D_\psi$. Indeed, as seen in panels 1.d and 2.d in Figs. 3 and 4, $D_\psi$ shows pronounced maxima near the phase values in which the mean velocity is minimal. This effect occurs both above and below the bifurcation, and is seen for both large and small noise levels. The slowing down of the systems in these regions is consistent with the phase functions having more densely packed isochrons, which in turn corresponds to large phase gradients. Large values of both the gradients $\nabla\Psi$ and the stationary density $P_0$ near low-velocity areas explain the large values of $D_\psi$ in these regions. These effects are also apparent in Eq. (35).

Finally, we comment the results of the reduction procedure applied to the MRT phase. By construction, the MRT phase defines sections with uniform mean return times. For this reason, one should not be surprised to find a constant drift term. In this case, all the variability in the velocity along the cycle is carried by the effective noise term $D_\Theta$. As for $D_\psi$, the collocation of high stationary density and large phase gradients leads to large values of the diffusion coefficient; cf. (38). We also see that the mean-return-time period $\overline{T}$ reflects the difference between regimes: $a_\theta = 2\pi/\overline{T}$ is smaller below bifurcation than above, meaning that $\overline{T}$ is larger below bifurcation than above.

## VI. CHECKING THE ACCURACY OF THE REDUCTION VIA ITS LONG-TERM STATISTICS

Our choice for the drift and effective noise coefficients of the reduced phase equation (25) ensures our reduction accurately captures the *short-term* ($\lim \mathrm{d}t \to 0$) statistics of the full phase evolution. However, a meaningful phase reduction should also be able to reliably capture the *long-term* (asymptotic) statistics of the evolution of the full system. For that reason, given a general phase mapping as in Eq. (23), we will consider the following statistics: the mean rotation rate

$$\omega^\phi_{\text{eff}} = \lim_{t\to\infty} \frac{1}{t}\langle \Phi_{\text{unwrapped}}(t) - \Phi_{\text{unwrapped}}(0)\rangle, \tag{41}$$

and the phase diffusion coefficient

$$D^\phi_{\text{eff}} = \lim_{t\to\infty} \frac{1}{2t}\left\langle \left[\Phi_{\text{unwrapped}}(t) - \Phi_{\text{unwrapped}}(0) - \omega^\phi_{\text{eff}} t\right]^2\right\rangle, \tag{42}$$

where we note that both statistics require using the *unwrapped* phases as done in (31). We will numerically compute those two quantities from ensemble of realizations of (i) the full phase mapping $\Phi(\mathbf{X}(t))$ [solution of Eq. (24)] and (ii) its corresponding self-contained phase reduction $\phi(t)$ [solution of Eq. (25)]. We consider that the closer the values of both statistics for the full and the reduced system, the more accurately our reduction captures the full dynamics.

Additionally, since the general phase reduction Eq. (25) is a 1D SDE with periodic drift and noise coefficients $a_\phi$ and $D_\phi$, we can use the results in [37], which give us the following

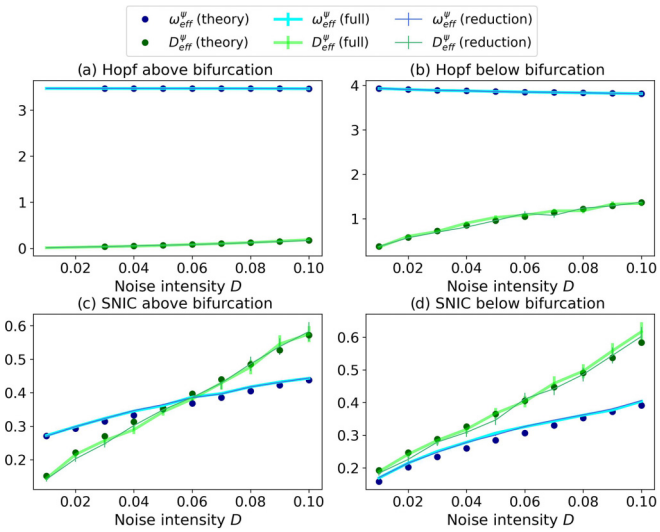


FIG. 6. Long-term statistics of the asymptotic phase $\psi$ as a function of the noise strength $D$. (a) Hopf bifurcation in the LC case; (b) Hopf bifurcation in the focus case; (c) SNIC in the LC case; (d) SNIC in the excitable case. We compute each statistic for the full phase Eq. (18) (thick line), its phase reduction Eq. (34) (narrow line), and the theoretical formulas, Eqs. (43) and (44) (dots). Bars width of one standard error. Results for the MRT are similar and can be found in Appendix C.

expressions for the mean rotation rate Eq. (41):

$$\omega^\phi_{\text{eff}} = \frac{2\pi\left(1 - e^{V(2\pi)}\right)}{\int_0^{2\pi} I_+(\tilde\phi)\,\mathrm{d}\tilde\phi/\sqrt{D_\phi(\tilde\phi)}}, \tag{43}$$

and the phase diffusion coefficient Eq. (42),

$$D^\phi_{\text{eff}} = \frac{4\pi^2 \int_0^{2\pi} I_-(\tilde\phi) I_+^2(\tilde\phi)\,\mathrm{d}\tilde\phi/\sqrt{D_\phi(\tilde\phi)}}{\left[\int_0^{2\pi} I_+(\tilde\phi)\,\mathrm{d}\tilde\phi/\sqrt{D_\phi(\tilde\phi)}\right]^3}, \tag{44}$$

where

$$V(\phi) = -\int_0^\phi \frac{a_\phi(\tilde\phi)}{D_\phi(\tilde\phi)}\,\mathrm{d}\tilde\phi$$

and

$$I_\pm(\phi) = \pm e^{\mp V(\phi)} \int_\phi^{\phi\pm 2\pi} \frac{e^{\pm V(\tilde\phi)}}{\sqrt{D_\phi(\tilde\phi)}}\,\mathrm{d}\tilde\phi.$$

The evaluation of the corresponding integrals is feasible as long as the noise intensity is not too small. Additional details regarding the numerical computation of Eqs. (41)–(44) can be found in the SM [29].

In Fig. 6 we show the long-term statistics of the full asymptotic phase $\Psi(\mathbf{X}(t))$ and of its corresponding reduction $\psi(t)$ as functions of the noise strength $D$. In general, we observe a good agreement between those quantities for both studied models. For the Hopf system, our phase reduction captures both the mean rotation rate $\omega^\psi_{\text{eff}}$ and the diffusion coefficient $D^\psi_{\text{eff}}$ of the full system in both the LC and quasicycle regimes [Figs. 6(a) and 6(b)]. We also observe a good agreement

for the SNIC bifurcation both above and below the bifurcation [Figs. 6(c) and 6(d)]. Appendix C shows that repeating these calculations for the full MRT phase mapping $\Theta(\mathbf{X}(t))$ and its corresponding reduction $\theta(t)$ yields a similar level of agreement.

## VII. INFERRING PHASE RESPONSE PROPERTIES

We will now show how our stochastic phase reduction framework can be applied to infer the phase response to weak external perturbations at linear order. In the case of a deterministic oscillator parameterized with phase $\vartheta$, the phase response to a weak perturbation can be linearized around the LC such that it is proportional to the gradient of the phase. This quantity is known as the *infinitesimal phase response curve* (iPRC) [38]

$$\mathrm{iPRC}(\vartheta) = \nabla\vartheta(\mathbf{x})|_{\mathbf{x}=\gamma(\vartheta)}, \tag{45}$$

where $\mathbf{x} = \gamma(\vartheta)$ is the parametrization of the LC.

The main obstacle in finding a stochastic analog of this quantity is the phase variability inherent to stochastic oscillators. As there is no LC, trajectories may visit any point $\mathbf{x}$ of the phase space with a given probability $P_0(\mathbf{x})$. As a consequence, perturbing the system at the same phase will generally yield different phase responses.

Consistent with our averaging approach to obtain a one-dimensional phase description, we postulate that, given a phase mapping $\Phi(\mathbf{x})$ as the one defined in (23), a meaningful curve describing the mean response properties of the system can be obtained by averaging its gradient along a given isochron. We call this quantity the *averaged iPRC (aiPRC)*, and can write it either in integral form

$$\mathrm{aiPRC}(\phi) = \int_{\mathbf{x}\in\mathcal{I}_\phi} \nabla\Phi(\mathbf{x}(\phi,\eta))\bar{P}_0(\eta|\phi)\,d\eta \tag{46}$$

or as an average across realizations

$$\mathrm{aiPRC}(\phi) = \langle\nabla\Phi(\mathbf{X}(t))\rangle_{\Phi(\mathbf{X}(t))=\phi} \tag{47}$$

with both (46) and (47) satisfying $\mathrm{aiPRC}(\phi) = \mathrm{aiPRC}(\phi + 2\pi)$. We remark that for systems with an underlying LC, in the vanishing noise limit ($D \to 0$), $P_0(\mathbf{x}) \to 0\ \forall\mathbf{x} \notin$ LC, and so (46) and (47) converge to the deterministic iPRC (45). We show that our aiPRC provides the expected phase shift $\Delta\Phi(\phi) = \phi_{\mathrm{new}} - \phi$ of an oscillator subjected to a weak external pulse $\boldsymbol{\epsilon}\delta(t - t_0)$ as

$$\Delta\Phi(\phi) \approx \boldsymbol{\epsilon}\cdot\mathrm{aiPRC}(\phi). \tag{48}$$

In Fig. 7 we plot the aiPRC and compare it with numerical estimates of the average phase response, obtained by perturbing the system with a weak pulse at random phases, computing the individual phase shifts and binning the responses by phase. For each bin, we compute the average response using the circular mean [39]. In Fig. 7(a) we compute the aiPRC for the Hopf normal form in the LC case (above the bifurcation). In this case, we observe that the aiPRC shows the characteristic sinusoidal Type II shape. Interestingly, a similar sinusoidal structure is found for the Hopf normal form for $\delta = -0.01$, when no LC exists. We note, however, that the amplitude of the mean response is larger in the quasicycle case than in the LC case. In this last case, the phase gradients dramatically increase near the origin where the probability density has a pronounced maximum. For the SNIC in the LC case [Fig. 7(c)], we observe that the aiPRC exhibits a Type I structure, very similar to the deterministic case (see [40] where this particular example is studied). Interestingly, this structure is not much altered when the same object is studied below the bifurcation. We observe similar behavior for the aiPRC computed for the MRT phase (see Appendix C).

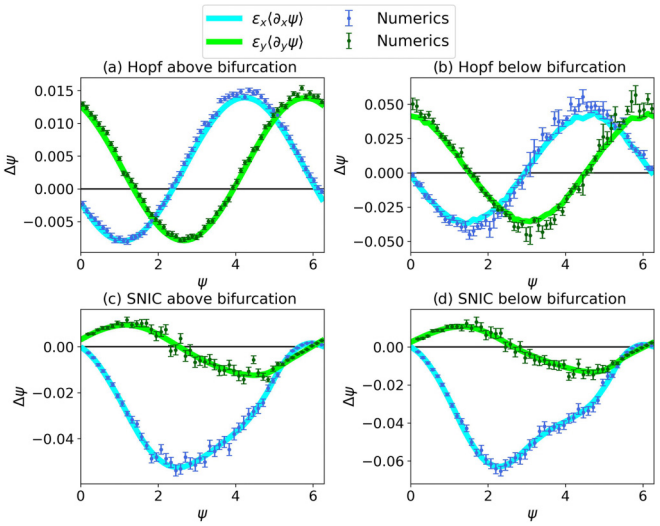


FIG. 7. Averaged iPRCs for the asymptotic phase $\psi$. Blue: response to a pulse in the $X$ direction (amplitude $\epsilon_x$). Green: response to a pulse in the $Y$ direction ($\epsilon_y$). (a) Hopf above bifurcation; (b) Hopf below bifurcation; (c) SNIC above bifurcation; (d) SNIC below bifurcation. External level of noise used for all systems: $D = 0.01$; pulse amplitudes: $\epsilon_x = \epsilon_y = 0.01$. Bar width of one standard error.

## VIII. EXTENSION BEYOND TWO DIMENSIONS

For the sake of illustration, the models we considered thus far were two-dimensional stochastic oscillators. We now discuss how our framework applies beyond the planar case ($n > 2$). As discussed in Sec. IV, given a phase observable $\Phi(\mathbf{x})$ as in (25), its respective isochrons correspond to $n-1$ dimensional manifolds, which we assume can be parameterized by $n-1$ amplitude-like variables. For example, in the case $n = 3$, the isochrons form 2D manifolds in the phase space, each of which can be parameterized by two amplitude-like variables (see [41–43] for examples of three-dimensional isochrons and examples of such a parametrization for deterministic oscillators).

To show how our method extends to higher dimensional oscillators, we consider a stochastic version of the three-dimensional Morris-Lecar neuron model, with slow delayed rectifier $K^+$ and subthreshold currents $I_{K,\mathrm{dr}}$ and $I_{\mathrm{sub}}$:

$$dV = \frac{1}{C}\Bigg[I_{\mathrm{ext}} - \overbrace{g_{\mathrm{fast}}m_\infty(V)(V-E_{\mathrm{Na}})}^{I_{Na}} - \overbrace{g_{K,\mathrm{dr}}Y(V-E_K)}^{I_{K,\mathrm{dr}}} - \overbrace{g_{\mathrm{sub}}Z(V-E_{\mathrm{sub}})}^{I_{\mathrm{sub}}} - \overbrace{g_L(V-E_L)}^{I_L}\Bigg]dt + \sqrt{\frac{2D}{C}}\,dW(t)$$

$$dY = \phi_Y \frac{Y_\infty(V) - Y}{\tau_Y(V)}\, dt,$$
$$dZ = \phi_Z \frac{Z_\infty(V) - Z}{\tau_Z(V)}\, dt. \tag{49}$$

A variant of this model was introduced in [44] using an Ornstein-Uhlenbeck process noise source as the stimulating current. Here, for simplicity, we adopt uncorrelated white noise in place of the OU process. We choose the parameter values such that the neuron model exhibits class I excitability, i.e.. the system is poised at the edge of a SNIC bifurcation (see Appendix D for the numerical values of parameters). The input-current fluctuations $\sqrt{2D}\xi(t)$ trigger noise-induced oscillations of the neuronal activity. This means that the duration between two spiking events, the interspike interval (ISI), is a random variable.

Computing $\mathcal{L}^\dagger$ for higher dimensional systems is a nontrivial issue. To do so, we use generator extended dynamic mode decomposition (gEDMD), a recently developed data-driven method that relies on the knowledge of the underlying SDE to compute an approximation of $\mathcal{L}^\dagger$, its eigenvalues and its eigenfunctions, on an arbitrary basis of functions, in a judiciously chosen domain of the phase space [18]. Using this approach allows us to perform our stochastic phase reduction using the stochastic asymptotic phase $\Psi(\mathbf{x})$. To lower the computational cost of calculating the eigenfunctions of $\mathcal{L}^\dagger$ in higher dimensions, we use a long realization of the system to identify a region $\mathcal{R}$ of the phase space in which the oscillator typically resides (roughly corresponding to where the stationary density exceeds some small threshold) and compute an approximation of $\mathcal{L}^\dagger$, its eigenfunctions, and thus of $\Psi(V, Y, Z)$, valid within this region. We then compute the self-contained phase reduction $\psi(t)$ in (34) by generating many trajectories of system (49). Next we compute the drift $a_\psi$ and effective noise $D_\psi$ coefficients by averaging those many trajectories via Eqs. (30) and (32). To evaluate the quality of the reduction, we compute the long-term statistics, as done in Sec. VI. We refer the reader to the SM [29] for additional numerical details.

We can further use gEDMD to compute the averaged iPRCs discussed in Sec. VII. Given that gEDMD approximates $Q_{\lambda_1}$ on a judiciously chosen basis of functions $\{F_i(\mathbf{x})\}$ such that

$$Q^*_{\lambda_1}(\mathbf{x}) \approx \sum_i v_i F_i(\mathbf{x}), \tag{50}$$

$v_i \in \mathbb{C}$, then we can also approximate its gradient as

$$\nabla Q^*_{\lambda_1}(\mathbf{x}) \approx \sum_i v_i \nabla F_i(\mathbf{x}). \tag{51}$$

In light of the identity

$$\nabla\Psi \equiv \nabla \arctan\left(\frac{\mathrm{Im}\left[Q^*_{\lambda_1}\right]}{\mathrm{Re}\left[Q^*_{\lambda_1}\right]}\right)$$
$$= \frac{\mathrm{Re}\left[Q^*_{\lambda_1}\right]\nabla\mathrm{Im}\left[Q^*_{\lambda_1}\right] - \mathrm{Im}\left[Q^*_{\lambda_1}\right]\nabla\mathrm{Re}\left[Q^*_{\lambda_1}\right]}{\left|Q^*_{\lambda_1}\right|^2}, \tag{52}$$

the gradient of $\psi$ may be approximated by way of (50) and (51). Then, using the expression for $\nabla\Psi(\mathbf{x})$ in (52) and assuming ergodicity, we can compute the aiPRC from time averages of realizations of the system using Eq. (47).

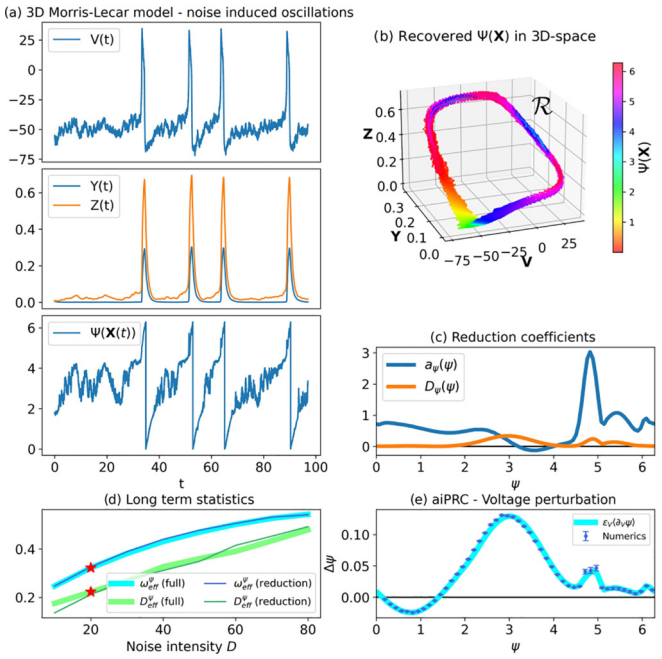


FIG. 8. Asymptotic phase for the 3D Morris-Lecar model. (a) Typical realization of system [49] and recovered phase by means of gEDMD. (b) Recovered asymptotic phase $\psi$ in the 3D phase space. Most realizations are confined around the region $\mathcal{R}$. (c) Reduction coefficients. (d) Long-term statistics. (e) Averaged iPRCs for the asymptotic phase for $\epsilon_V = 1$. Noise intensity in panels (a), (b), (c), and (e): $D = 20$ (highlighted with a red star in panel d).

Figure 8 displays the results of our gEDMD-based method. Figure 8(a) shows a typical realization of system [49] and the corresponding stochastic asymptotic phase $\Psi(V(t), Y(t), Z(t))$. The phase captures both the oscillatory nature of the neuron's activity, and the fluctuations which lead to irregular oscillations. Figure 8(b) shows the asymptotic phase function $\Psi(\mathbf{x})$ in the three-dimensional phase space recovered via gEDMD. The phase increases steadily, on average, with traces of noise-induced backtracks. Figure 8(c) shows the coefficients $a_\psi$ and $D_\psi$ of the reduced dynamics. As in the SNIC case, either in the LC regime with large noise levels or in the excitable regime, (cf. Fig. 3, panel 2.d, and Fig. 4, panels 1.d and 2.d, respectively) $a_\psi$ shows a small region of negative mean drift. In addition, for a narrow range of phase around $\psi \approx 4.5$–5, there is a pronounced peak in $a_\psi$, corresponding approximately to the triggering and upswing of the spike. In contrast, the effective noise term $D_\psi$ is maximal near $\psi \approx \pi$, corresponding to the regions of irregular voltage fluctuation during the plateau between spikes. Figure 8(d) shows that the reduced phase equation captures the long-term dynamics of the full system evolution, which we interpret as a sign that the reduced SDE is a satisfactory description of system [49]. Figure 8(e) compares the expected phase response with the response obtained via direct perturbation. The responses match, showing that the procedure leading to the formula $\nabla\Psi$ derived from (50)–(52) allows us to predict the response of the oscillator to an external pulse.

## IX. DISCUSSION

### A. Summary

In this work, we developed a generalized self-contained stochastic phase reduction framework. Specifically, we provided a method for finding an approximate, self-contained phase reduction of stochastic oscillators subjected to Gaussian white noise. To illustrate our framework, we considered two mappings $\Phi\colon(\mathbf{x}) \in \mathbb{R}^n \to \mathbb{T} \equiv [0, 2\pi)$, namely, the "mean-return-time" phase $\Theta(\mathbf{x})$ introduced in [11] and the "stochastic asymptotic phase" $\Psi(\mathbf{x})$ introduced in [13]. Throughout this work, we focused on examples of two-dimensional stochastic oscillators. However, the framework can be applied to $n$-dimensional systems: as a proof of concept, we applied our reduction procedure to a three-dimensional neuron model. For simplicity's sake, we considered only systems with additive noise in our applications. However, the analytical expressions for the reduction procedure are valid for the multiplicative noise case, which will be explored in more detail in future work.

Our reduction is built by considering the short-term dynamics of the full phase variable. In order to test the accuracy of our reduction, we considered two well-known long-term statistics: the mean rotation $\omega^{\phi}_{\text{eff}}$, and the diffusion coefficient $D^{\phi}_{\text{eff}}$. We consider the reduction to be better, the closer the agreement of these two statistics for (i) the full phase system and (ii) its reduced version. As previously mentioned, we have studied our reduction method for two different phase functions $\Theta(\mathbf{x})$ and $\Psi(\mathbf{x})$. Although the long-term statistics of a given oscillator are necessarily identical for both *full* phase mappings, we have not found significant differences on the asymptotic statistics when considering a particular phase for reducing. Indeed, as we observe in Figs. 6, 8, 12, the long-term accuracy of both reductions, $\psi(t)$ and $\theta(t)$, remains good for all levels of noise in the range considered.

In contrast to the long-term behavior, we find differences between the considered phase mappings when it comes to the *short-term* behavior. Indeed, we have found important differences in the drift functions, $a_\theta$ and $a_\psi$. The MRT phase has a constant drift term, so the phase dependence of its dynamics resides entirely in the effective noise term $\sqrt{2D_\theta(\theta)}$. By contrast, the stochastic asymptotic phase, shows a nonconstant drift term. As we have shown in Fig. 5, this variable drift term, at small noise, reflects important *dynamical* information about the system, namely, the transition from an excitable to an oscillatory regime. Under strong noise conditions, however, zeros in the drift function can be observed both above and below the deterministic bifurcation point.

A way to understand this difference between drift functions is by relating our approach to the noise-induced frequency shift (NIFS) phenomenon [5]: In a deterministic LC oscillator with phase $\vartheta$, adding white noise typically causes a shift in the average frequency [45]. The new average frequency is given by the ensemble average, $\overline{\omega} = \langle\dot{\vartheta}\rangle$. For a general stochastic oscillator, we see that, by construction, the MRT phase takes the effect of noise on the frequency into account by setting its instantaneous frequency to the average frequency: $a_\theta(\theta) = \overline{\omega} = \frac{2\pi}{\overline{T}}$, for all $\theta$. By contrast, the asymptotic phase has an additional degree of variability, as it has an instantaneous average frequency value $a_\psi(\psi)$ which need not equal $\overline{\omega}$. Thus, the asymptotic phase keeps track of finer details arising from the interaction between noise and deterministic dynamics, at the cost of added complexity in the equation.

### B. Future directions

In this paper, we have applied our method to systems whose SDE was known. However, both the MRT phase and the stochastic asymptotic phase can be extracted from data. For example, the original procedure to extract the MRT was built upon an iterative method that can accommodate both simulated and real-world data [11]. The stochastic asymptotic phase was first extracted from data by fitting the oscillatory-exponential asymptotic decay of the probability density to its stationary state [13]. The family of dynamic mode decomposition (DMD) methods, such as gEDMD, based on an eigenfunction decomposition of the Koopman operator (which is closely related to the Kolmogorov backwards operator for stochastic systems) offer an alternative approach to obtaining these functions (see [18]). Thus, as we have shown in Sec. VIII by means of gEDMD, they can allow one to recover an estimation of the spectral properties of $\mathcal{L}^\dagger$ from data, most particularly of the $Q^*_{\lambda_1}$ eigenfunction that carries the stochastic asymptotic phase; cf. [46]. This connection would allow application of our framework to real world oscillatory data, to be explored in future work.

In the deterministic case, adding an amplitude variable can extend the domain of accuracy of the phase description [20,42,47,48]. We believe our construction may benefit from a similar approach. Recently, the spectral analysis of $\mathcal{L}^\dagger$ has been extended to provide an analog of the so-called amplitude coordinates [21,49]. In related work, it has been shown that a different observable, the slowest decaying complex eigenfunction $Q^*_{\lambda_1}$ of the Kolmogorov backwards operator, yields a universal description of stochastic oscillators [50]. This complex phase function, $Q^*_{\lambda_1}$, allows comparison of stochastic oscillators regardless of their underlying oscillatory mechanism [50]. Written in polar form, the complex phase function $Q^*_{\lambda_1} = ue^{i\psi}$ defines both a notion of phase $\psi \in [0, 2\pi)$ and an amplitude $u$ that captures the concentration or coherence of an oscillator's probability density. Both the stochastic analogues of the phase-amplitude description and the complex phase ideas appear as interesting targets for future research in the field of stochastic dynamics [16,17,51–54].

An additional interesting question arising from this work is the exploration of the *averaged infinitesimal phase response curve (aiPRC)* function defined in Sec. VII. We have shown that it provides a meaningful estimation of the average phase response of a stochastic oscillator to a small pulselike perturbation. Being able to compute the average response of stochastic oscillators to external perturbations by means of the aiPRC is a first step towards the analysis of complex noisy oscillatory phenomena, such as synchronization among oscillators connected on networks [2,34,55]. In the past, defining those phenomena, such as noisy phase and frequency synchronization [56], or noise-enhanced phase locking [57], required using a deterministic notion of phase, such as the Hilbert phase, and extending it to the noisy case. The work we put forward in this paper builds upon recent notions of stochastic phase [11,13]. Thus, obtaining a reduction for those

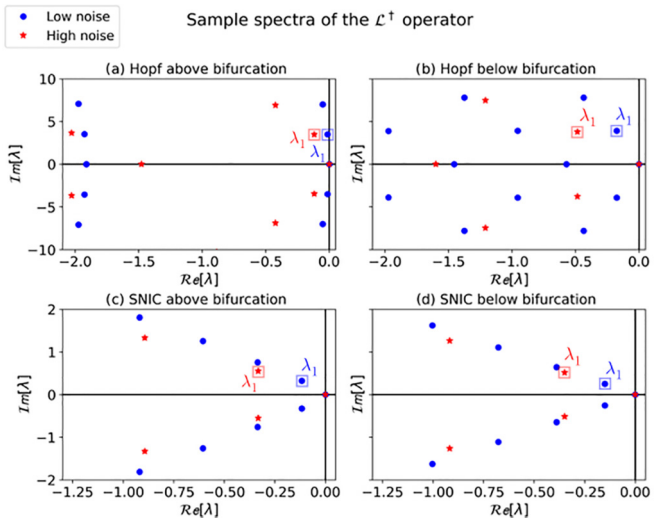


FIG. 9. Spectra of the backwards operator $\mathcal{L}^\dagger$ for the planar models. We plot the spectra of $\mathcal{L}^\dagger$ for external noise amplitudes $D = 0.01$ (blue dots) and $D = 0.08$ (red stars). The box indicates the nontrivial eigenvalue $\lambda_1$ with least real part and positive imaginary part. We indicate the values of $\lambda_1$ for weak (large) noise, respectively. (a) $\lambda_1 = -0.01 + i3.5$, ($\lambda_1 = -0.12 + i3.48$); (b) $\lambda_1 = -0.18 + i3.92$, ($\lambda_1 = -0.48 + i3.78$); (c) $\lambda_1 = -0.12 + i0.32$, ($\lambda_1 = -0.33 + i0.55$); (d) $\lambda_1 = -0.15 + i0.25$, ($\lambda_1 = -0.35 + i0.51$).

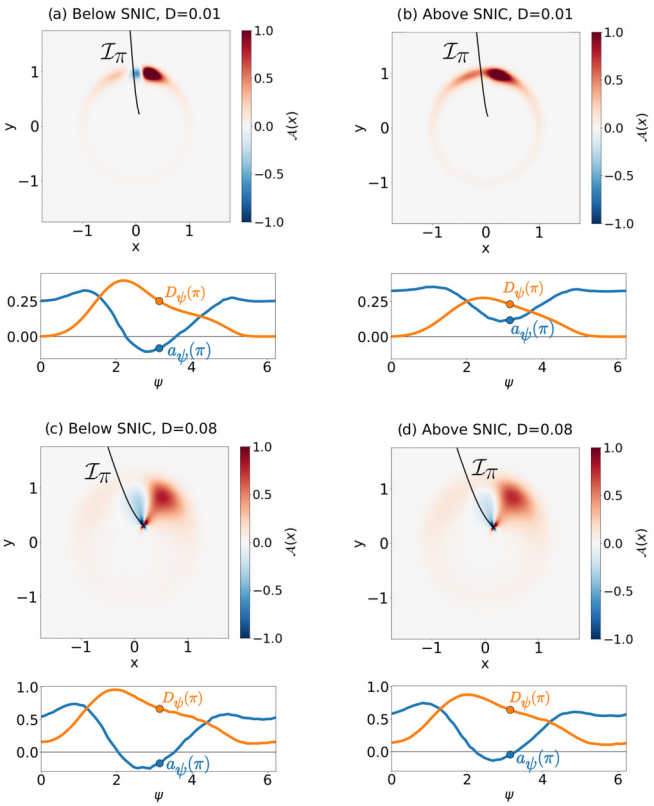


FIG. 10. SNIC drift speed variations. For small ($D = 0.01$) and large ($D = 0.08$) levels of noise, we plot the function $\mathcal{A}(\mathbf{x})$ in (B2) both below ($m = 0.999$) and above ($m = 1.03$) the SNIC bifurcation in system (40). We also plot the corresponding drift $a_\psi(\psi)$ (blue) and diffusion $D_\psi(\psi)$ (orange) functions shown in Figs. 3 and 4. In black, we show the asymptotic phase isochron $\mathcal{I}_\pi$ corresponding to the phase $\psi = \pi$ and highlight the corresponding drift and diffusion terms recovered when averaging along $\mathcal{I}_\pi$.

stochastic phases will allow us to revisit those earlier results in a purely stochastic setting. Moreover, Adams and MacLaurin have recently proposed a formal approach to deriving a self-contained stochastic differential equation for what they term the "isochronal phase"; for systems that have a particular invariant manifold structure (such as system with an underlying LC) see [58]. Application of their methods, drawn from rigorous analysis of stochastic partial differential equations, to the examples we present here, is an interesting opportunity for future investigation.

## ACKNOWLEDGMENTS

This research was funded by Agence Nationale pour la Recherche (ANR-17-EURE-0017, ANR-10IDEX-0001-02), ENS, CNRS, and INSERM. This work was supported in part by (i) NSF Grant No. DMS-2052109, (ii) the Oberlin College Department of Mathematics, and (iii) the National Science Foundation under Grant No. DMS-1929284 while the author P.J.T. was in residence at the Institute for Computational and Experimental Research in Mathematics in Providence, RI, during the "Math + Neuroscience: Strengthening the Interplay Between Theory and Mathematics" program. P.H. acknowledges support from École Doctorale Frontières de l'Innovation en Recherche et Éducation and UPC ALECTORS 23. A.P.C. is a Serra Húnter Fellow and acknowledges support from the Spanish Ministry of Science and Innovation (Project No. PID2021-124047NB-I00).

## DATA AVAILABILITY

All code used to produce the results shown in this work is available at [60]. The gEDMD code was made publicly available by the authors of [18] at [61].

## APPENDIX A: EXAMPLES OF EIGENVALUE SPECTRA FOR ROBUSTLY OSCILLATORY SYSTEMS

In this Appendix we show the spectra of the Hopf and SNIC models in the main text for the considered levels of noise $D = 0.01$ and $D = 0.08$. As Fig. 9 shows, in all the cases there exists a nontrivial eigenvalue of $\mathcal{L}^\dagger$ with least negative real part $\lambda_1 = \mu_1 + i\omega_1$, which is complex valued ($\omega_1 > 0$) and unique. Hence, as pointed out in [13] and explained in Sec. III A, the slowest decaying mode associated with $\lambda_1$ is complex, so one can extract the stochastic asymptotic phase $\Psi(\mathbf{x})$ from the backward eigenfunction $Q_{\lambda_1}(\mathbf{x})$. We also note that, consistent with the observations of [30], in the Hopf case we observe a qualitative change in the shape of the principal eigenvalue family, which lies approximately along a parabola above the bifurcation, and approximately along a straight line, as part of a checkerboard-like grid, below the bifurcation.

## APPENDIX B: ILLUSTRATING THE SNIC CASE

We provide additional details regarding the shapes of the drift term $a_\psi$ for the SNIC model that we observe in Figs. 3 and 4. As discussed in Sec. IV C, the evolution law

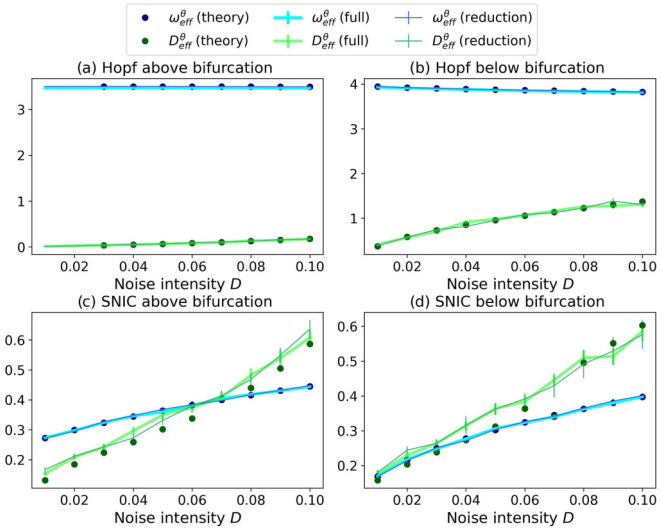


FIG. 11. Long-term statistics of the MRT phase $\Theta(\mathbf{x})$ as a function of the noise strength $D$. (a) Hopf bifurcation in the LC case; (b) Hopf bifurcation in the focus case; (c) SNIC in the LC case; (d) SNIC in the excitable case. We compute each statistic for the full phase Eq. (22) (thick line), its phase reduction Eq. (36) (narrow line), and the theoretical formulas Eqs. (43) and (44) (dots). Error bars span one standard error.

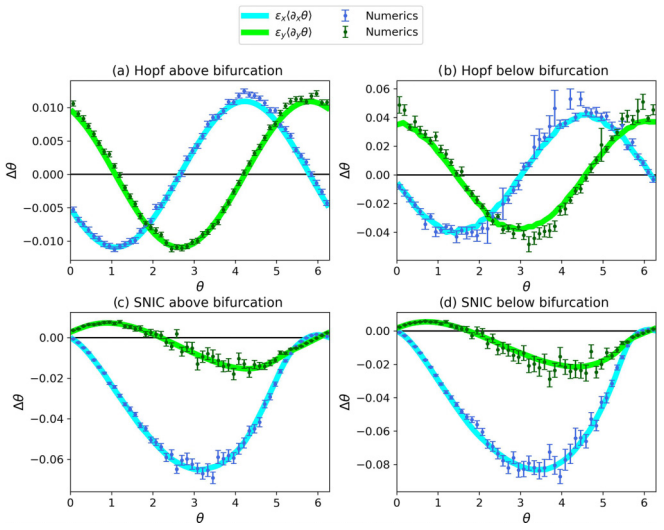


FIG. 12. Averaged iPRCs for the MRT phase $\Theta(\mathbf{x})$. Blue: response to a pulse in the $X$ direction (amplitude $\epsilon_x$); Green: response to a pulse in the $Y$ direction ($\epsilon_y$). (a) Hopf above bifurcation; (b) Hopf below bifurcation; (c) SNIC above bifurcation; (d) SNIC below bifurcation. External level of noise used for all systems: $D = 0.01$; pulse amplitudes: $\epsilon_x = \epsilon_y = 0.01$. Error bars span one standard error.

of $\mathrm{d}\Psi(\mathbf{X}(t))$ in (18) yields a drift term $a_\psi(\psi)$ of the form

$$a_\psi(\psi) = \omega_1 - \int_{\mathbf{x}\in\mathcal{I}_\psi} \bar{P}_0(\eta|\psi)\Omega(\mathbf{x})d\eta, \tag{B1}$$

with $\Omega(\mathbf{x})$ defined in (18). To study the values for $a_\psi$ in the SNIC case, we define the following function:

$$\mathcal{A}(\mathbf{x}) = P_0(\mathbf{x})(\omega_1 - \Omega(\mathbf{x})), \tag{B2}$$

where we weight the term $\omega_1 - \Omega(\mathbf{x})$ by the stationary density $P_0(\mathbf{x})$, making explicit the contribution of each point $\mathbf{x} \in \mathcal{D}$ when computing the average in Eq. (B1).

We summarize our results in Fig. 10, in which we plot $\mathcal{A}(\mathbf{x})$ for the SNIC model. For the sake of clarity, we also include the corresponding drift and diffusion terms $a_\psi$ and $D_\psi$ shown in Figs. 3 and 4.

In the small noise case ($D = 0.01$), below the bifurcation [Fig. 10(a)], we observe the function $\mathcal{A}(\mathbf{x})$ to be mainly positive with the exception of a tiny area in which $\mathcal{A}(\mathbf{x}) < 0$. This area is the one to which we find the isochrons $\mathcal{I}_\psi$ such that $a_\psi(\psi) < 0$ (as is the case for, e.g., with $\psi = \pi$). By contrast, above the bifurcation, we find $\mathcal{A}(\mathbf{x}) \geqslant 0\,\forall\mathbf{x} \in \mathcal{D}$, such that $a_\psi(\psi) > 0\,\forall\psi \in \mathbb{T}$.

By contrast, as we increase the external level of noise, we lose this smooth transition from a $a_\psi$ with negative values to a fully positive $a_\psi$: for $D = 0.08$, the drift function displays a range of phases in which $a_\psi$ is negative both above and below the bifurcation. The emergence of "noise-induced" zeros in the drift term above the bifurcation as the noise increases can be illustrated by means of $\mathcal{A}(\mathbf{x})$. Indeed, for $D = 0.08$, we find $\mathcal{A}(\mathbf{x})$ to be very similar both above and below the bifurcation [see Figs. 10(c) and 10(d)].

## APPENDIX C: MRT EXTRA RESULTS: LONG-TERM STATISTICS AND aiPRCs

### 1. MRT long-term statistics

Following Sec. VI, we compute the mean rotation rate $\omega^\theta_{\text{eff}}$ in (41) and the diffusion coefficient $D^\theta_{\text{eff}}$ in (42) by means of (i) the full mapping $\Theta(\mathbf{X}(t))$ solution of Eq. (22) and (ii) the self-contained reduction $\theta(t)$ solution of Eq. (36). Additionally, as was done in Sec. VI, since the general phase reduction is a 1D SDE with periodic drift and noise coefficients, we use the results in [37] to compute the mean rotation rate and the diffusion coefficient by means of the theoretical expressions Eqs. (43) and (44). Results are shown in Fig. 11. As for the stochastic asymptotic phase results in Fig. 6, we find a very good level of agreement between the values of $\omega^\theta_{\text{eff}}$ and $D^\theta_{\text{eff}}$ for the full and the reduced phase dynamics. *MRT averaged iPRC:* Following Sec. VII, we compute the *averaged infinitesimal Phase Response Curve* (aiPRC) for the MRT phase $\nabla\Theta(\mathbf{x})$ as an average across realizations (47). Results are shown in

TABLE I. Parameters of the 3D Morris-Lecar model in (49).

| | |
|---|---|
| $m_\infty(V)$: $0.5[1 + \tanh(\frac{V-\beta_m}{\gamma_m})]$ | $\beta_m$: $-1.2$ mV, $\gamma_m$: 18 mV |
| $Y_\infty(V)$: $0.5[1 + \tanh(\frac{V-\beta_Y}{\gamma_Y})]$ | $\tau_Y(V)$: $1/\cosh(\frac{V-\beta_Y}{2\gamma_Y})$ |
| $\beta_Y$: -10 mV, $\gamma_Y$: 10 mV | $\phi_Y$: 0.15 |
| $Z_\infty(V)$: $0.5[1 + \tanh(\frac{V-\beta_Z}{\gamma_Z})]$ | $\tau_Z(V)$: $1/\cosh(\frac{V-\beta_Z}{2\gamma_Z})$ |
| $\beta_Z$: $-21$ mV, $\gamma_Z$: 15 mV | $\phi_Z$: 0.5 |
| $E_{\text{Na}}$: 50 mV | $E_{\text{K}}$: $-100$ mV |
| $E_{\text{L}}$: $-70$ mV | $E_{\text{sub}}$: 50 mV |
| $g_{\text{fast}}$: 20 mS/cm$^2$ | $g_{\text{K, dr}}$: 20 mS/cm$^2$ |
| $g_{\text{sub}}$: 2 mS/cm$^2$ | $g_{\text{L}}$: 2 mS/cm$^2$ |
| C: 1 $\mu$F/cm$^2$ | $I_{\text{ext}}$: 29 $\mu$A/cm$^2$ |

Fig. 12 and present a good agreement between predicted and measured responses.

## APPENDIX D: MORRIS-LECAR PARAMETERS

The parameters used for the 3D Morris-Lecar model are given in Table I.


[1] A. Pikovsky, J. Kurths, M. Rosenblum, and J. Kurths, *Synchronization: A Universal Concept in Nonlinear Sciences*, Cambridge Nonlinear Science Series Vol.12 (Cambridge University Press, Cambridge, 2003).

[2] F. C. Hoppensteadt and E. M. Izhikevich, *Weakly Connected Neural Networks*, edited by J. E. Marsden, L. Sirovich, and F. John, Applied Mathematical Sciences (Springer New York, New York, 1997), Vol. 126.

[3] A. T. Winfree, *The Geometry of Biological Time*, edited by J. E. Marsden, S. Wiggins, and L. Sirovich, Interdisciplinary Applied Mathematics (Springer New York, New York, 2001), Vol. 12.

[4] G. B. Ermentrout, B. Beverlin, T. Troyer, and T. I. Netoff, The variance of phase-resetting curves, J. Comput. Neurosci. **31**, 185 (2011).

[5] K. Yoshimura and K. Arai, Phase reduction of stochastic limit cycle oscillators, Phys. Rev. Lett. **101**, 154101 (2008).

[6] J.-N. Teramae, H. Nakao, and G. B. Ermentrout, Stochastic phase reduction for a general class of noisy limit cycle oscillators, Phys. Rev. Lett. **102**, 194102 (2009).

[7] P. C. Bressloff and J. N. MacLaurin, A variational method for analyzing stochastic limit cycle oscillators, SIAM J. Appl. Dyn. Syst. **17**, 2205 (2018).

[8] J. MacLaurin, Phase reduction of waves, patterns, and oscillations subject to spatially extended noise, SIAM J. Appl. Math. **83**, 1215 (2023).

[9] B. Lindner, J. García-Ojalvo, A. Neiman, and L. Schimansky-Geier, Effects of noise in excitable systems, Phys. Rep. **392**, 321 (2004).

[10] J. Guckenheimer, Isochrons and phaseless sets, J. Math. Biol. **1**, 259 (1975).

[11] J. T. C. Schwabedal and A. Pikovsky, Phase description of stochastic oscillations, Phys. Rev. Lett. **110**, 204102 (2013).

[12] A. Cao, B. Lindner, and P. J. Thomas, A partial differential equation for the mean–return-time phase of planar stochastic oscillators, SIAM J. Appl. Math. **80**, 422 (2020).

[13] P. J. Thomas and B. Lindner, Asymptotic phase for stochastic oscillators, Phys. Rev. Lett. **113**, 254101 (2014).

[14] A. S. Powanwe and A. Longtin, Amplitude-phase description of stochastic neural oscillators across the Hopf bifurcation, Phys. Rev. Res. **3**, 033040 (2021).

[15] J. Zhu, Y. Kato, and H. Nakao, Phase dynamics of noise-induced coherent oscillations in excitable systems, Phys. Rev. Res. **4**, L022041 (2022).

[16] C. W. Gardiner, *Handbook of Stochastic Methods for Physics, Chemistry, and the Natural Sciences*, 3rd ed., Springer Series in Synergetics (Springer-Verlag, Berlin, 2004).

[17] N. Črnjarić Žic, S. Maćešić, and I. Mezić, Koopman operator spectrum for random dynamical systems, J. Nonlinear Sci. **30**, 2007 (2020).

[18] S. Klus, F. Nüske, S. Peitz, J.-H. Niemann, C. Clementi, and C. Schütte, Data-driven approximation of the Koopman generator: Model reduction, system identification, and control, Physica D **406**, 132416 (2020).

[19] A. Pérez-Cervera, B. Lindner, and P. J. Thomas, Quantitative comparison of the mean–return-time phase and the stochastic asymptotic phase for noisy oscillators, Biol. Cybern. **116**, 219 (2022).

[20] S. Shirasaka, W. Kurebayashi, and H. Nakao, Phase-amplitude reduction of limit cycling systems, in *The Koopman Operator in Systems and Control*, Lecture Notes in Control and Information Sciences, edited by A. Mauroy, I. Mezić, and Y. Susuki (Springer International Publishing, Cham, 2020), Vol. 484, pp. 383–417.

[21] Y. Kato, J. Zhu, W. Kurebayashi, and H. Nakao, Asymptotic phase and amplitude for classical and semiclassical stochastic oscillators via Koopman operator theory, Mathematics **9**, 2188 (2021).

[22] N.B. In the Koopman operator literature the term "mode" connotes the projections of observables on eigenfunctions (I. Mezić, personal communication).

[23] Unlike the stochastic asymptotic phase, the MRT phase requires the operator $\mathcal{L}^\dagger$ to be strongly elliptic [59].

[24] The exact formulation of the jump boundary conditions is given by

$$\lim_{\varepsilon\to 0^+} T(K(\phi+2\pi-\varepsilon,\boldsymbol{\eta}))-T(K(\phi+\varepsilon,\boldsymbol{\eta}))=\overline{T}, \quad \text{(D1)}$$

where $K(\phi,\boldsymbol{\eta})$ refers to the parametrization defined in (26).

[25] Similarly, the SDE for the "variational phase" derived in [8] is not self-contained.

[26] R. Friedrich and J. Peinke, Description of a turbulent cascade by a Fokker-Planck equation, Phys. Rev. Lett. **78**, 863 (1997).

[27] C. Touya, T. Schwalger, and B. Lindner, Relation between cooperative molecular motors and active Brownian particles, Phys. Rev. E **83**, 051913 (2011).

[28] M. Ragwitz and H. Kantz, Indispensable finite time corrections for Fokker-Planck equations from time series data, Phys. Rev. Lett. **87**, 254501 (2001).

[29] See Supplemental Material at http://link.aps.org/supplemental/10.1103/PhysRevResearch.7.033052 for details on the numerical methods used to compute all relevant quantities derived in the manuscript.

[30] A. Tantet, M. D. Chekroun, H. A. Dijkstra, and J. D. Neelin, Ruelle-Pollicott resonances of stochastic systems in reduced state space. Part II: Stochastic Hopf bifurcation, J. Stat. Phys. **179**, 1403 (2020).

[31] R. D. Hempstead and M. Lax, Classical noise. VI. Noise in self-sustained oscillators near threshold, Phys. Rev. **161**, 350 (1967).

[32] O. V. Ushakov, H.-J. Wünsche, F. Henneberger, I. A. Khovanov, L. Schimansky-Geier, and M. A. Zaks, Coherence resonance near a Hopf bifurcation, Phys. Rev. Lett. **95**, 123903 (2005).

[33] F. Jülicher, K. Dierkes, B. Lindner, J. Prost, and P. Martin, Spontaneous movements and linear response of a noisy oscillator, Eur. Phys. J. E **29**, 449 (2009).

[34] J. Cabral, F. Castaldo, J. Vohryzek, V. Litvak, C. Bick, R. Lambiotte, K. Friston, M. L. Kringelbach, and G. Deco, Metastable oscillatory modes emerge from synchronization in the brain spacetime connectome, Commun. Phys. **5**, 184 (2022).

[35] P. J. Thomas and B. Lindner, Phase descriptions of a multidimensional Ornstein-Uhlenbeck process, Phys. Rev. E **99**, 062221 (2019).
[36] H. A. Brooks and P. C. Bressloff, Quasicycles in the stochastic hybrid Morris-Lecar neural model, Phys. Rev. E **92**, 012704 (2015).
[37] B. Lindner and L. Schimansky-Geier, Noise-induced transport with low randomness, Phys. Rev. Lett. **89**, 230602 (2002).
[38] G. B. Ermentrout and D. H. Terman, *Mathematical Foundations of Neuroscience*, Interdisciplinary Applied Mathematics (Springer New York, New York, 2010), Vol. 35.
[39] K. V. Mardia and P. E. Jupp, *Directional Statistics*, new ed., Wiley Series in Probability and Statistics (Wiley, Chichester, 2000).
[40] A. Guillamon and G. Huguet, A computational and geometric approach to phase resetting curves and surfaces, SIAM J. Appl. Dyn. Syst. **8**, 1005 (2009).
[41] A. Mauroy and I. Mezić, Global computation of phase-amplitude reduction for limit-cycle dynamics, Chaos **28**, 073108 (2018).
[42] A. Pérez-Cervera, T. M-Seara, and G. Huguet, Global phase-amplitude description of oscillatory dynamics via the parameterization method, Chaos **30**, 083117 (2020).
[43] D. Wilson, Phase-amplitude reduction far beyond the weakly perturbed paradigm, Phys. Rev. E **101**, 022220 (2020).
[44] S. A. Prescott, Y. De Koninck, and T. J. Sejnowski, Biophysical basis for three distinct dynamical mechanisms of action potential initiation, PLoS Comput. Biol. **4**, e1000198 (2008).
[45] J. M. Newby and M. A. Schwemmer, Effects of moderate noise on a limit cycle oscillator: Counterrotation and bistability, Phys. Rev. Lett. **112**, 114101 (2014).
[46] P. Melland and R. Curtu, Attractor-like dynamics extracted from human electrocorticographic recordings underlie computational principles of auditory bistable perception, J. Neurosci. **43**, 3294 (2023).
[47] O. Castejón, A. Guillamon, and G. Huguet, Phase-amplitude response functions for transient-state stimuli, J. Math. Neurosci. **3**, 13 (2013).
[48] B. Monga, D. Wilson, T. Matchen, and J. Moehlis, Phase reduction and phase-based optimal control for biological systems: A tutorial, Biol. Cybern. **113**, 11 (2019).
[49] A. Pérez-Cervera, B. Lindner, and P. J. Thomas, Isostables for stochastic oscillators, Phys. Rev. Lett. **127**, 254101 (2021).
[50] A. Pérez-Cervera, B. Gutkin, P. J. Thomas, and B. Lindner, A universal description of stochastic oscillators, Proc. Natl. Acad. Sci. USA **120**, e2303222120 (2023).
[51] H. Risken, *The Fokker-Planck Equation: Methods of Solution and Applications*, edited by H. Haken, Springer Series in Synergetics (Springer, Berlin, 1996), Vol. 18.
[52] I. Mezić, Spectral properties of dynamical systems, model reduction and decompositions, Nonlinear Dyn. **41**, 309 (2005).
[53] M. D. Chekroun, A. Tantet, H. A. Dijkstra, and J. D. Neelin, Ruelle–Pollicott resonances of stochastic systems in reduced state space. Part I: Theory, J. Stat. Phys. **179**, 1366 (2020).
[54] F. Hummel, P. Ashwin, and C. Kuehn, Reduction methods in climate dynamics—A brief review, Physica D **448**, 133678 (2023).
[55] R. Nicks, R. Allen, and S. Coombes, Insights into oscillator network dynamics using a phase-isostable framework, Chaos **34**, 013141 (2024).
[56] J. A. Freund, L. Schimansky-Geier, and P. Hänggi, Frequency and phase synchronization in stochastic systems, Chaos **13**, 225 (2003).
[57] A. Neiman, A. Silchenko, V. Anishchenko, and L. Schimansky-Geier, Stochastic resonance: Noise-enhanced phase coherence, Phys. Rev. E **58**, 7118 (1998).
[58] Z. P. Adams and J. MacLaurin, The isochronal phase of stochastic PDE and integral equations: Metastability and other properties, J. Diff. Equ. **414**, 773 (2025).
[59] W. C. H. McLean, *Strongly Elliptic Systems and Boundary Integral Equations* (Cambridge University Press, Cambridge, 2000).
[60] https://github.com/PHouzel/stocha-phase-red
[61] https://github.com/sklus/d3s/